NOVEL COLLOIDAL SYSTEMS FOR THE INVESTIGATION OF BINARY MIXTURES

ARTHUR LAKES LIBRARY
COLORADO SCHOOL OF MINES
GOLDEN, CO 80401

by

Pinsuda Viravathana

ProQuest Number: 10796893

All rights reserved

INFORMATION TO ALL USERS
The quality of this reproduction is dependent upon the quality of the copy submitted.

In the unlikely event that the author did not send a complete manuscript
and there are missing pages, these will be noted. Also, if material had to be removed,
a note will indicate the deletion.

ProQuest 10796893

Published by ProQuest LLC (2019). Copyright of the Dissertation is held by the Author.

All rights reserved.
This work is protected against unauthorized copying under Title 17, United States Code
Microform Edition © ProQuest LLC.

ProQuest LLC.
789 East Eisenhower Parkway
P.O. Box 1346
Ann Arbor, MI 48106 – 1346

Copyright by Pinsuda Viravathana 2001

All Rights Reserved

A thesis submitted to the Faculty and Board of Trustees of the Colorado School of Mines in partial fulfillment of the requirements for the degree of Doctor of Philosophy (Chemical Engineering and Petroleum Refining).

Golden, Colorado

Date 4/6/01

Signed: _____

Pinsuda Viravathana

Approved: _____

Dr. David W.M. Marr

Thesis Advisor

Golden, Colorado

Date: 4/6/01

_____

Dr. James F. Ely

Professor and Head

Department of Chemical Engineering

and Petroleum Refining

ABSTRACT

To develop systems for the experimental investigation of binary systems with short and long-ranged interactions, two novel colloidal systems have been synthesized. One is a "core-shell" system, when the colloid has a high-index titania core and a lower index silica shell. By index-matching the solvent for silica in a mixture of silica and silica-coated titania colloids, the core can be manipulated by optical trapping techniques, allowing the study of colloidal phase behavior. The other system developed is based on "contrast variation". To use scattering techniques to investigate binary systems, there must be two particle kinds present, each having a slightly different index of refraction. Aluminosilicate colloids were therefore synthesized with a slightly higher index of refraction than silica. By index-matching silica, the aluminosilicate distribution could be determined; similarly, by index matching for aluminosilicate, the silica distribution could be extracted. In addition it was observed that by changing solvent, attractive interactions could be introduced to these mixtures leading to different scattering behavior. Results from these experimental studies were compared to results from thermodynamic calculations. With the development of these novel experimental model systems, new routes are now available for the investigation of binary mixture phase and nucleation behavior.

TABLE OF CONTENTS

LIST OF FIGURES

LIST OF TABLES

ACKNOWLEDGMENTS

I would like to start by showing my appreciation to my advisor, Dr. David W.M. Marr, for the guidance and support over the years. I thank him for always being available and patient, also giving freedom on my study. I would like to thank the late Dr. M. Sami Selim for the useful suggestions through particle syntheses and Dr. Kelly T. Miller for his helpful discussions on particle characterizations. Also, I would like to thank the members of my committee, Dr. James F. Ely, Dr. Kim R. Williams, and Dr. David T. Wu.

For the time spent at Mines, I would like to thank the Marr group for their help and support, which makes me feel very lucky to be part of the group. I also would like to express my appreciation to the Colorado School of Mines, Chemical Engineering and Petroleum Refining Department for giving me the opportunity to pursue my studies, and to my instructors and friends for all the remarkable knowledge and memories.

I am grateful to Royal Thai Government for the scholarship throughout the years. And, I would like to express my thankfulness to Thai Students at Mines for being supportive and like a family while providing me joyful moments.

I would like to thank my grandpa for being my role model.

I would like to thank my grandma, mom, and dad for their unconditional love and support. I finally thank my brothers, Pasna and Polrit, for all the encouragement they have given me, and sister-like, Nuta, Areeyata, Kanjanee, and Sirirat for their support.

For my grandparents and my parents.

CHAPTER 1

INTRODUCTION

1.1 Importance of Research

Industrial processes typically involve mixtures of many components. This can be by design, as is often the case in reaction engineering, or undesirable when small amounts of impurities may be present. Crystallization is one example process where the behavior of components of low concentration may be critical. A better control of the crystallization process could allow engineers to improve material strength or produce extremely pure single crystals. It may even allow researchers to develop methods for the prevention of crystallization; one example is protein crystallization which is the major cause of some diseases such as sickle cell anemia and cataracts.

Crystallization from the melt is a complicated process however. To form ordered structures from a homogeneous fluid, a critical number of particles must first gather into a cluster before crystals can begin to grow [1]. This phenomenon is called nucleation. A better understanding of crystallization processes that include nucleation requires investigations at the molecular level however. For this reason, and despite many years of study, a great deal is unknown about the nucleation process.

Despite the difficulties, one can begin by predicting where crystallization will occur, for which mixture phase diagrams are extremely useful. Though relatively easy for single component systems, understanding and predicting the phase behavior of multicomponent mixtures can be extremely difficult. To understand these complex systems, one approach is to begin with less complicated systems and develop a fundamental understanding of observed trends. To simplify the complexity of multicomponent systems, we will focus our discussions primarily on mixtures of two species, known as a binary component system.

During nucleation, individual particles must first come together in order to form a critical nucleus for further crystal growth. It is clear that interactions between individual particles, either attractive or repulsive, will play a large role in this process. To simplify interactions between components, one can begin with purely repulsive interactions as a base for investigations of more complicated interactions.

From the literature, it is apparent that many researchers have investigated the phase behavior of pure, binary, and multicomponent systems, including both theoretical and experimental studies. Though much is known about the phase behavior of purely repulsive systems, little has been done on systems with more complicated interactions. For binary systems with relatively simple attractive interactions, theoretical approaches have been used to investigate phase behavior; however, there has not yet been confirmation with simple experimental models of these systems.

Our investigations are focused on developing experimental model systems that can facilitate the investigation of binary systems with simple interactions between individual species. Our experimental models will mimic hard spheres, one of the simplest realistic models where the interaction potential between each particle is purely repulsive. In addition, with these same model systems, one will be able to study binary systems with more complicated interactions. For example, to modify the hard sphere model, a short-ranged attraction can be introduced experimentally, allowing an approximation of the theoretical model known as adhesive spheres. More complicated interactions can also be introduced, including long-ranged interactions. For these studies, we have developed experimental model systems with a range of repulsive interaction several times the sphere radius.

Why study binary mixtures?

Theoretical studies of multicomponent systems for even simple models can be extremely difficult. In order to understand the behavior of such complicated systems, techniques for the study of simpler systems must be first developed. In this spirit, a number of studies have been performed to characterize the structural and thermodynamic properties of single-component systems with hard sphere interactions [2, 3]. For single component systems, previous studies have determined the phase diagram [4], and the equation of state [5, 6], via theoretical and experimental approaches. For binary systems,

a number of theoretical studies of phase behavior have been conducted, including Monte Carlo simulation [7, 8, 9], molecular dynamics simulation [9, 10], liquid state theory [11, 12], and density functional theory [13]. Hard sphere mixtures have also been investigated using experimental approaches [14, 15, 16].

For more complicated interactions such as the adhesive sphere system (*i.e.*, when attractions are added to the hard sphere system), studies have been conducted via both theoretical and experimental approaches. However, for mixtures of such systems, there have been few thermodynamic phase behavior studies and no experimental investigations. Many questions remain regarding the phase behavior of binary systems with simple attractive interactions; therefore, we choose to develop systems with simple repulsive and attractive interactions for experimental investigations.

Why use colloids?

We use colloids to represent theoretical systems for a number of reasons. They can be synthesized in a wide range of sizes, they are large enough to be visible under a microscope; they are kinetically slow, and one can easily and indirectly manipulate colloidal interactions. To alter these interactions, polymer chains can be grafted onto the surface, minimizing the influence of dispersion forces between colloidal particles at short-range. Without grafted polymers, colloidal surface charge can be used to introduce a long-ranged repulsion. Besides manipulating the colloidal surface charge, solvents can

be used to change colloidal interactions. When dispersed in a good solvent, grafted polymer chains prefer to interact with the solvent leading to a net repulsive interaction between particles. When suspended in a poor solvent, grafted polymer chains prefer to interact among themselves introducing an effective attractive interaction. Colloidal interactions can also be tuned by varying ionic strength. When the ionic concentration is increased, ions screen the surface charge causing a decrease in electrostatic repulsions.

In addition to indirect manipulation by varying colloidal surface chemistry or dispersing solvent however, colloidal particles can be directly controlled. Through the use of optical trapping techniques, colloidal particles can be manipulated within a suspension directly and, with a microscope and image analysis techniques, the resulting colloidal behavior can be investigated.

1.2 Research Objectives

Our goal is to develop experimental models of binary systems using colloids to represent theoretical models with short and long-ranged interactions. Using these model systems, one will be able to investigate the structure and phase behavior of binary mixtures. Although real processes involve more complicated systems, such studies will provide a good base case that can be later modified for more detailed interactions.

For some studies, we need to prepare colloidal systems that are appropriate for use with a specific technique. One approach we use is optical trapping, where one can

directly manipulate individual colloids and for which there must be a mismatch in the index of refraction between the solvent and the colloidal particles. However, if we wish to minimize dispersion forces and have short-ranged interactions, there must be an index-match between particles and solvent. Therefore, for binary studies using optical trapping techniques, two colloidal systems must be synthesized, one of which has a core with a different index of refraction than its shell; we call this a "core-shell" system. In order to pursue binary studies, interactions between different particles would be altered by varying solvent or manipulating surface charges. Optical trapping will still be feasible due to the mismatch in refractive index between the core and solvent.

In a "core-shell" system, when two different kinds of particles are dispersed in index-matching solvents, only the core having a different in index of refraction will be seen via the optical microscope as shown in Figure 1-1. The core-shell particles can then be manipulated, moved around the suspension, or arranged in various patterns and sizes, as illustrated in Figure 1-2. By turning the beam on and off, the stability of such patterns can be determined and the associated phase behavior inferred. In addition, it is clear that such an approach could be used for the investigation of nucleation in binary mixtures.

The other technique we propose is light scattering. In order to perform binary studies using this approach, there must be two particle types having a slightly different index of refraction. If this difference is too great, multiple scattering occurs which prevents determination of colloidal structure. After manipulating the interactions

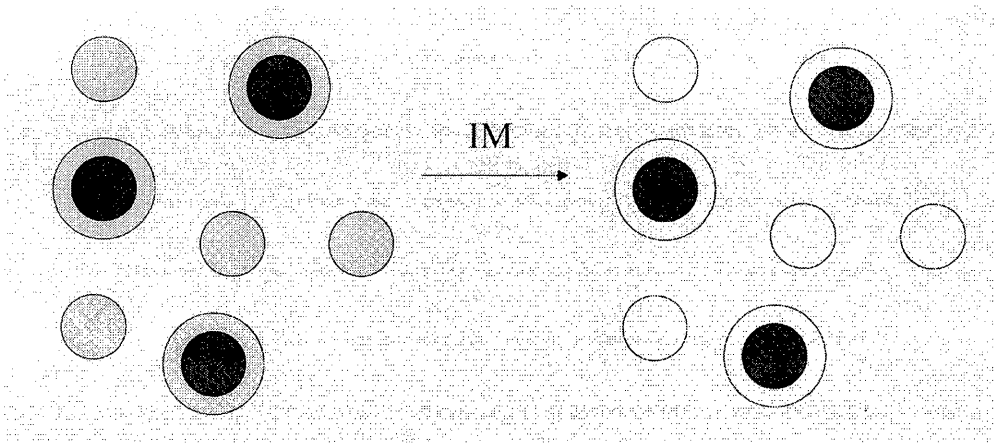

Figure 1-1 Core-shell approach IM = index matching.

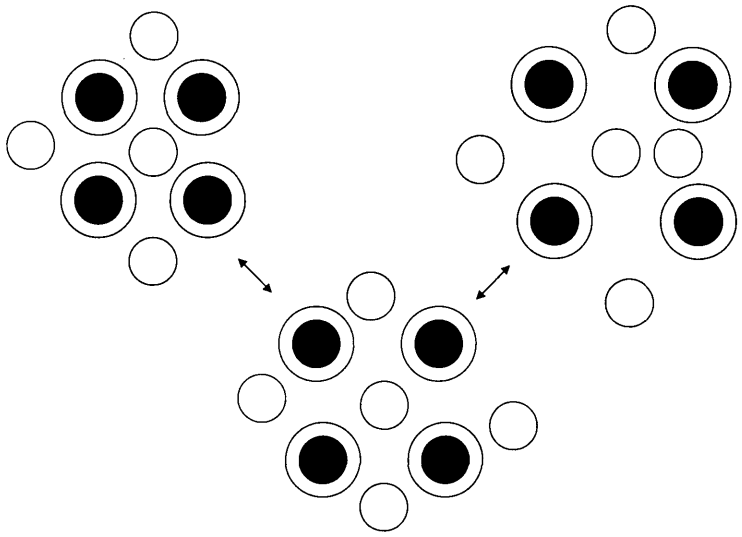

Figure 1-2 Scaling the optical traps for stability investigation.

between particles, index matching for one species allows extraction of information on the behavior of the other. Since there must be some contrast in the system in order to use this tool, we call this approach "contrast variation".

In a "contrast variation" approach for binary systems, once particles 1 are index-matched by the solvent, only particles 2 will scatter and information on the particle 2 distribution can be obtained. By varying the solvent mixture ratio, particles 2 can be index-matched and the particle 1 distribution can be determined. From both contributions, the intercorrelations between particles 1 and 2 can be extracted as illustrated in Figure 1-3.

With development of these experimental systems, there will be new routes available for the investigation of binary mixture phase and nucleation behavior. Such studies will eventually lead to investigations with more complicated interactions and a higher number of components.

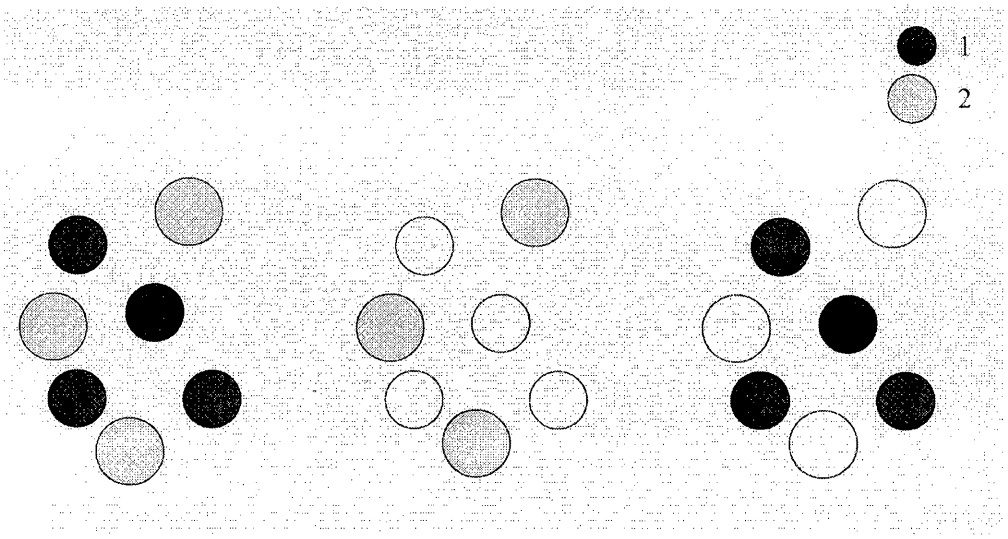

Figure 1-3 Contrast variation approach.

CHAPTER 2

BACKGROUND AND LITERATURE REVIEW

2.1 Fundamental Principles of Colloidal Science

Colloidal systems can be defined as a mixture of dispersed particles of one phase in a second continuous phase. The continuous phase can be gas, liquid, or solid and the dispersed phase can be any macromolecular particles of size between approximately 1 nm and 10 μm. Examples of two-phase colloidal systems are shown in Table 2-1. Colloidal particles are also defined on the basis of their affinity for the fluid in which they are dispersed. Lyophilic systems favor the solvent and lyophobic systems do not. If the solvent is water, the term hydrophilic and hydrophobic are commonly used. Example lyophilic colloids include soluble macromolecular materials of colloidal dimensions, such as synthetic polymers and proteins. A number of examples of lyophobic colloids are shown in Table 2-1. Our studies are concerned with systems where the dispersed phase is solid and the continuous phase is liquid, including both aqueous and non-aqueous solvents.

The behavioral characteristics of dispersed phase colloidal systems are controlled by the physical and chemical properties of colloidal materials, and are important in many aspects of industrial processes. Dispersions of solid in liquid can be found in numerous

process technologies such as suspension and gelation. To understand how dispersed matter behaves; studies at the microscopic level must be done.

Table 2-1 Summary of two-phase colloidal systems [17].

Dispersion Medium	**Dispersed Phase**	**Example**
Gas	Liquid	Fog, Mist, Aerosol
Gas	Solid	Smoke, Aerosol
Liquid	Gas	Foam
Liquid	Liquid	Emulsion
Liquid	Solid	Sol, Colloidal Solution, Gel, Suspension
Solid	Gas	Solid Foam
Solid	Liquid	Gel, Solid Emulsion
Solid	Solid	Alloy

The field of colloid and surface science is focused on the desire to understand and control processes that involve dispersed matter. Those involved in process design require adequate description of dispersion characteristics that influence the manner in which colloidal materials are processed. Application of these concepts in dispersions will result in economical and efficient processes.

2.1.1 Particle-Particle Interactions

In real colloidal systems, there are several interparticle interactions that can play a role. These include charge-induced repulsive interactions and attractions due to van der Waals forces. In addition, steric stabilization can be used to minimize attractions between colloidal particles, allowing interactions between colloids to approach purely repulsive hard spheres.

2.1.1.1 Electrical Double Layer Mediated Repulsions

When charged groups, such as carbonyl and sulfonyl, are present at the surface of colloidal particles, Coulombic repulsions arise between like-charged groups. This repulsive behavior can be screened by counterions present in the medium that form electrical double layers surrounding the particles.

In an aqueous medium and depending on pH, colloidal particles have an electrical charge on the surface giving rise to a surface electrostatic potential. For spherical particles [18], solutions to the non-linearized Poisson-Boltzmann equation (Equation 2.1) for the diffuse layer around a sphere are non-analytical and must be numerically solved. The Poisson-Boltzmann equation can be expressed as:

$$\frac{1}{r^2}\frac{\partial}{\partial r}r^2\frac{\partial \psi}{\partial r} = \frac{2ezn_b}{\varepsilon\varepsilon_0}\sinh\left(\frac{ez\psi}{kT}\right) \qquad [2.1]$$

where,

$\psi = \psi_s$ at $r = a$ (for the constant potential solution)

$\psi \rightarrow 0$ at $r \rightarrow \infty$

a = the particle radius

ψ = the electrostatic potential

ψ_s = the sphere surface potential

ε = the permittivity, also called the dielectric constant, of the medium

ε_0 = the permittivity of a vacuum = 8.854×10^{-12} C^2/Nm^2

n_b = bulk ionic concentration

z = valency of the ions

e = the fundamental electronic charge = 1.60210×10^{-19} C

k = Boltzmann's constant = 1.38054×10^{-23} J/K

For thin double layers, $\kappa a >> 1$ and the interaction potential can be nondimensionalized with

$$\Psi = \frac{ez\psi}{kT} \qquad [2.2]$$

where κ^{-1} = the Debye-Huckel electrical double layer thickness

$$\kappa^{-1} = \left(\frac{\varepsilon \varepsilon_0 kT}{2e^2 z^2 n_b} \right)^{1/2} \qquad [2.3]$$

There are several approaches to evaluation of Equation 2.1 for two interacting spheres. These include the linearized Derjaguin approximation for constant potential and constant charge, linear superposition of a sphere, and superposition of thin double-layer spheres [18]. With the assumption of linear superposition [18], the solution leads to

$$U^{rep} = 4\pi\varepsilon\varepsilon_0\left(\frac{kT}{ze}\right)^2 \frac{a^2}{r}\Psi_s^{\,2}\exp(-\kappa(r-2a)) \qquad [2.4]$$

where

r - $2a$ = the separation between the surface of two spheres

From Equation 2.4, it can be seen that the repulsive interaction decays via the $\exp[\kappa(r-2a)]$ term, illustrating the importance of the double layer thickness, κ^{-1}. This shows that when the electrolyte concentration in the system is low, the electrostatic repulsion will be long-ranged. At high electrolyte concentrations however, ions will screen the repulsions and the repulsive interaction decays rapidly.

For asymmetrical spherical particles with radius a_1 and a_2, the electrostatic repulsion is given by Hogg [19] and Ottewill [20] via the following:

$$U^{rep}(r) = \frac{\pi\varepsilon\varepsilon_0 a_1 a_2}{4(a_1+a_2)}\left(\psi_{s1}^2+\psi_{s2}^2\right)\left[\left(\frac{2\psi_{s1}\psi_{s2}}{\psi_{s1}^2+\psi_{s2}^2}\right)\ln\left(\frac{1+\exp(-\kappa x)}{1-\exp(-\kappa x)}\right)+\ln(1-\exp(-2\kappa x))\right] \qquad [2.5]$$

where ψ_{s1} and ψ_{s2} are the surface potentials of spheres 1 and 2, and $x = r - (a_1+a_2)$

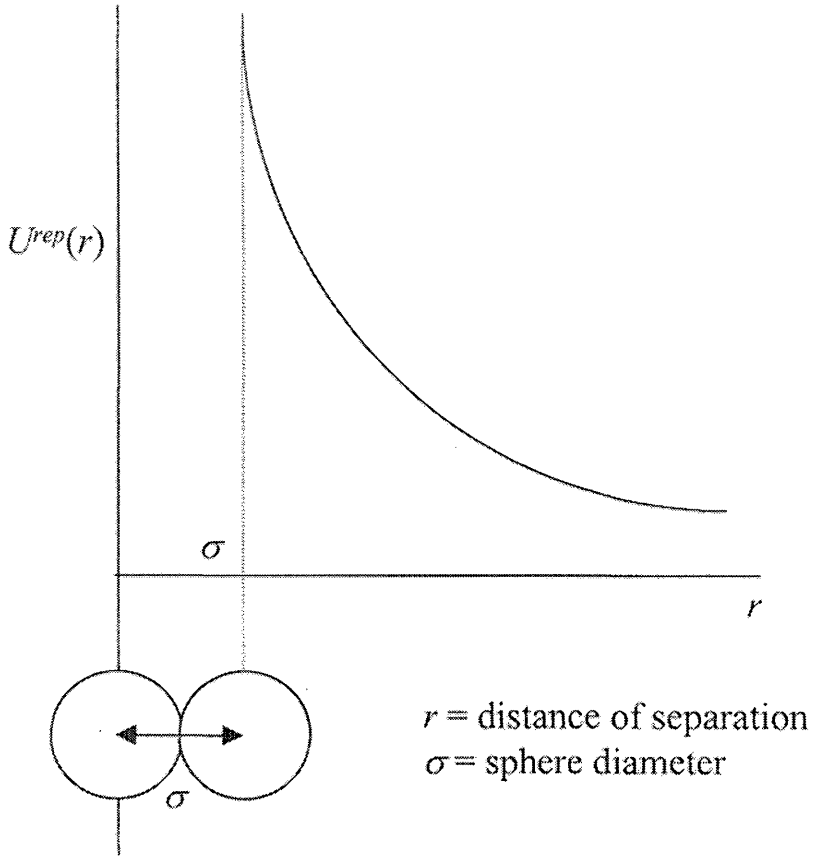

Figure 2-1 Electrostatic repulsion.

A plot of $U^{ep}(r)$ *vs.* r showing the electrostatic repulsion is shown in Figure 2-1. From the interaction potential, the force between the particles can be determined from the gradient, *i.e.* $F = -\vec{\nabla}U$. As can be seen from Figure 2-1, as these particles approach one another, repulsions become very strong, forcing the particles apart.

2.1.1.2 van der Waals Attractions

Between colloidal particles, van der Waals attractions (London forces) arise due to induced dipole-induced dipole interactions. Such attractions between atoms and molecules are relatively short-ranged (typically over a few-tenths of a nanometer). For colloidal particles however, every atom in one colloid attracts each atom in another; the net effect of which is to generate considerable long-range attractions between individual colloids. As a result, it is generally observed that uncharged colloidal particles will aggregate rapidly due to this interaction.

Mahanty & Ninham [18] have modeled dispersion interactions with the following:

$$U^{vdW}(r) = -A_{eff}(r-2a)H\left(\frac{r}{a}\right) \qquad [2.6]$$

where,

A_{eff} = effective Hamaker constant

$$= \frac{3}{4}kT\left(\frac{\bar{\varepsilon}(0)-\varepsilon(0)}{\bar{\varepsilon}(0)+\varepsilon(0)}\right)^2 + \frac{3h\omega}{32\sqrt{2}\pi}\frac{\left(\bar{n}_0^2-n_0^2\right)^2}{\left(\bar{n}_0^2+n_0^2\right)^{3/2}}F(H') \qquad [2.7]$$

and,

$$H' = n_0\left(\bar{n}_0^2 + n_0^2\right)^{1/2}\frac{(r-2a)\omega}{c} \qquad [2.8]$$

$$F(H') \approx \left[1+\left(\frac{\pi H'}{4\sqrt{2}}\right)^{3/2}\right]^{-2/3} \qquad [2.9]$$

$\bar{\varepsilon}$ (0), ε(0) = dielectric constant of sphere and medium

$\bar{n}_0, n_0$ = index of refraction of sphere and medium

ω = primary absorption frequency of colloid (for SiO_2 = 2.01×10^{16} rad/s)

h = Planck's constant = 6.6256×10^{-34} Js

For equal spheres of radius a,

$$H\left(\frac{r}{a}\right) = \left(\frac{2a^2}{r^2-4a^2} + \frac{2a^2}{r^2} + \ln\frac{r^2-4a^2}{r^2}\right)/6 \qquad [2.10]$$

and for asymmetric spheres of radius a_1 and a_2

$$H\left(\frac{r}{a}\right) = \left(\frac{2a_1a_2}{r^2-(a_1+a_2)^2} + \frac{2a_1a_2}{r^2-(a_1-a_2)^2} + \ln\frac{r^2-(a_1+a_2)^2}{r^2-(a_1-a_2)^2}\right)/6 \qquad [2.11]$$

The net interaction between two spheres with van der Waals attractions and a very short-ranged strong repulsion is shown in Figure 2-2.

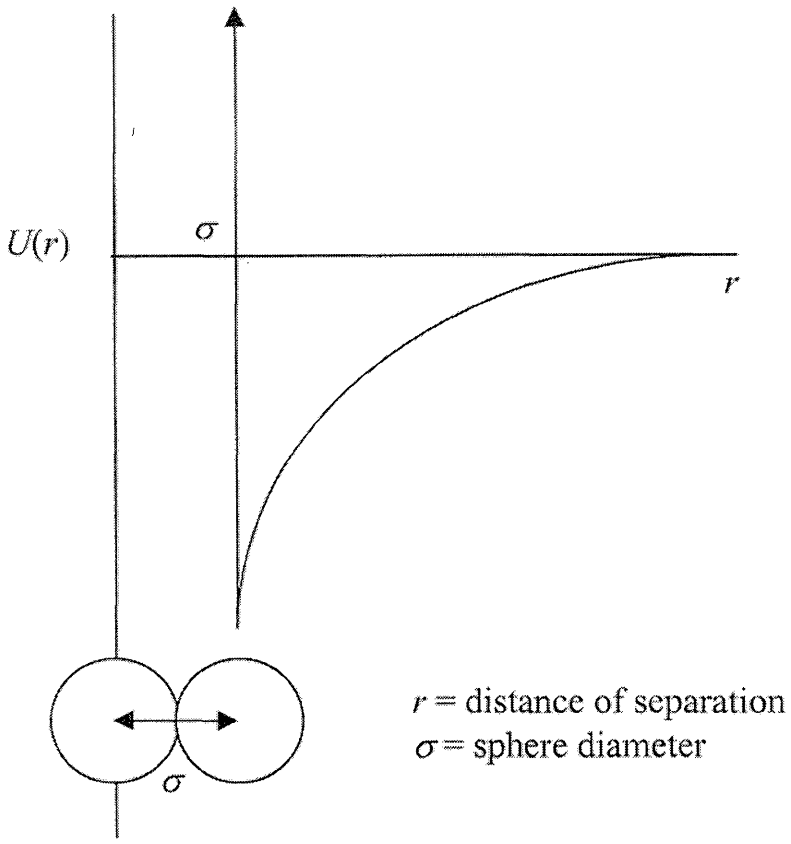

Figure 2-2 van der Waals attraction and short-ranged repulsion.

2.1.1.3 Steric Interactions

Polymers in solution also influence interactions between colloids via steric and depletion mechanisms. Steric stabilization of colloidal particles is accomplished when polymer chains are attached to particle surfaces via grafting or physical adsorption mechanisms. These polymer chains provide spacing between colloidal particles so that the interaction from the London forces is minimized. Depletion stabilization separates colloidal particles using free polymer molecules instead of those attached to the particle surface. In this case, free polymer molecules in solution screen the London interaction, resulting in the reduction of attractions between particles. Illustrations of steric and depletion stabilization are shown in Figure 2-3.

To achieve stable colloidal systems, either an individual method of stabilization or combinations of depletion, steric, and/or electrostatic stabilization may be applied. In our studies, we graft polymers to the sphere surface and use steric stabilization to minimize the attractive interaction in order to approximate hard and adhesive hard sphere behavior. The interaction potential between colloidal particles with grafted polymer chains can be modeled as [21]

$$U^{poly}(r)=\begin{cases}\infty & ,r<2a \\ U_0\left[-\ln(y)-\frac{9}{5}(1-y)+\frac{1}{3}(1-y^3)-\frac{1}{30}(1-y^6)\right] & ,2a<r<2(a+L) \\ 0 & ,r>2(a+L)\end{cases} \qquad [2.12]$$

where

$$y = \frac{r - 2a}{2L} \qquad [2.13]$$

and

$$U_0 = \left(\frac{\pi^3 L \sigma_P}{12 N_p l^2} k_B T \right) a L^2 . \qquad [2.14]$$

a = the particle radius

L = the polymer layer thickness

N_p = the number of segments in the polymer chain

l = the segment length

σ_p = the surface grafting density

by relating Derjaguin approximation to the interaction between flat, polymer coated surfaces. From Napper [22], the steric interaction is illustrated in Figure 2-4.

2.1.1.4 Combination of Interactions

In real colloidal dispersions, combinations of electrostatic, attractive, and steric interactions will be present and can lead to net interactions such as that shown in Figure 2-5.

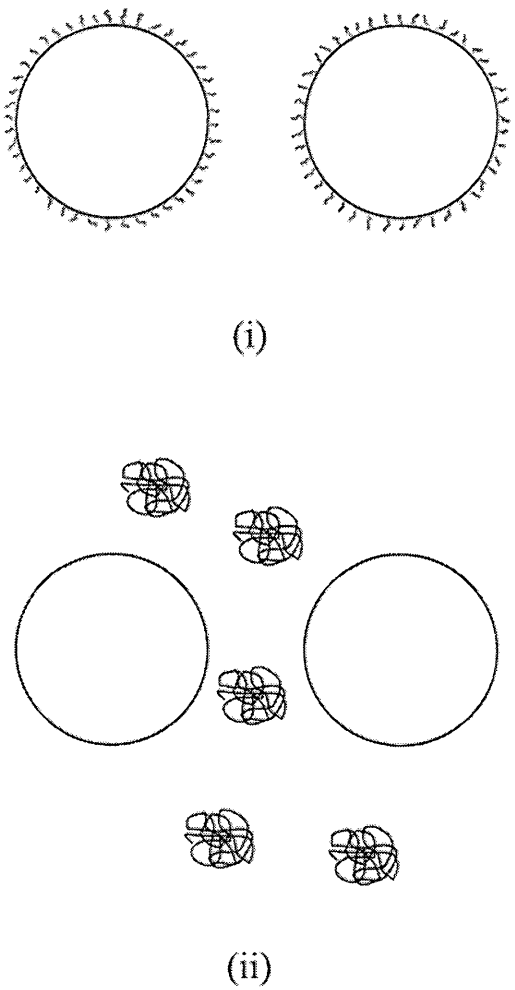

Figure 2-3 (i) Steric stabilization (ii) Depletion stabilization.

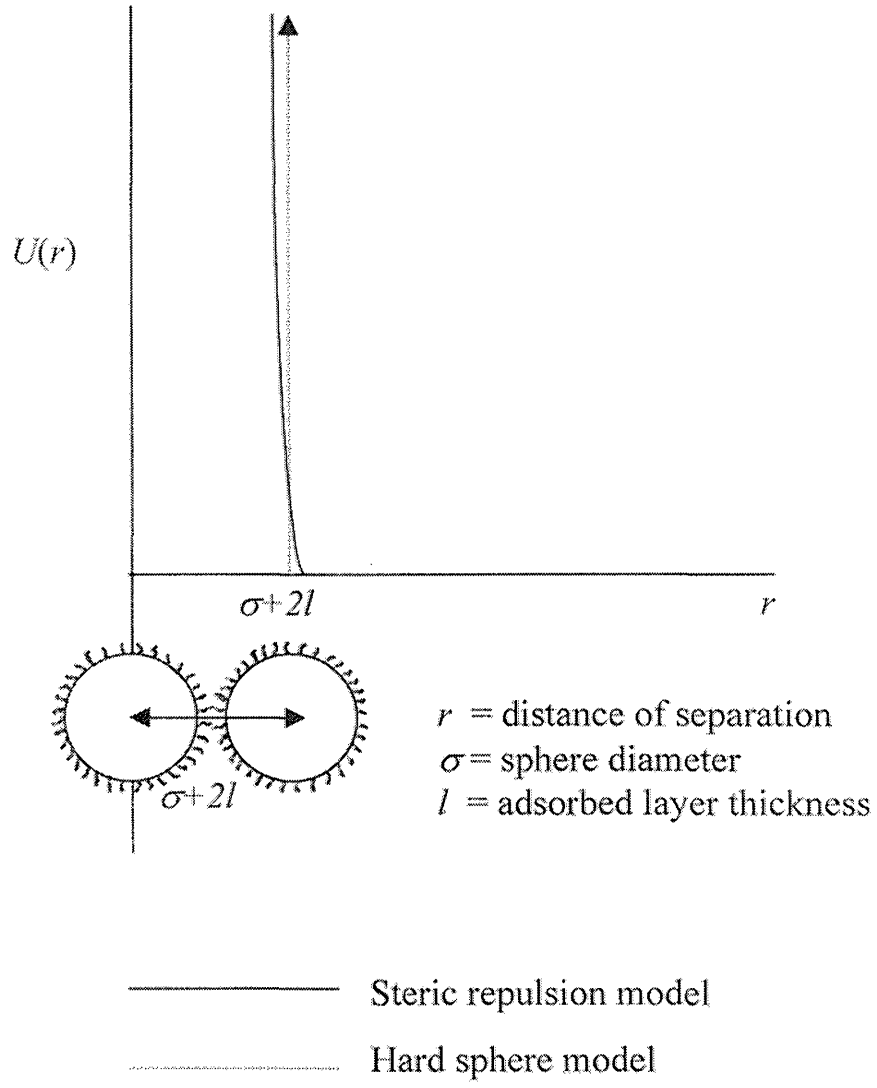

Figure 2-4 Steric interaction.

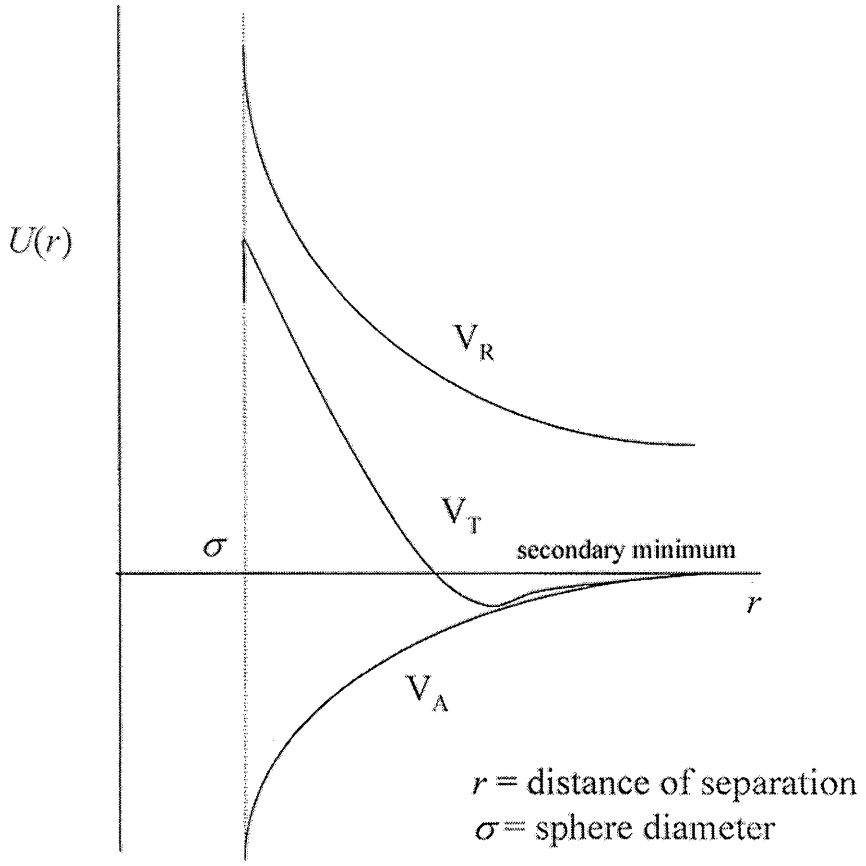

Figure 2-5 Interaction of charged sphere V_A = van der Waals interaction, V_R = Electrostatic interaction, and V_T = Total interaction (Adapted from [23]).

2.1.2 Particle Models

2.1.2.1 Hard Spheres

The hard sphere model is a purely theoretical one and consists of only repulsive interactions. The interaction potential in this system can be expressed as

$$U^{HS}(r) = \begin{cases} \infty & ,r \leq \sigma_{HS} \\ 0 & ,r > \sigma_{HS} \end{cases} \qquad [2.15]$$

where σ_{HS} = hard sphere diameter. From this, it can be seen that at close separation, the interaction between spheres is highly repulsive and at larger separations, the potential energy drops to zero. The interaction between hard spheres is illustrated in Figure 2-6.

If one wishes to approximate this hard sphere model using colloidal systems, particles must be prepared with purely repulsive interactions at close separation. Two commonly used synthetic approaches for producing hard sphere particles involve sterically stabilized silica and poly(methyl methacrylate) particles, a review of which will be presented in Section 2.3.1.

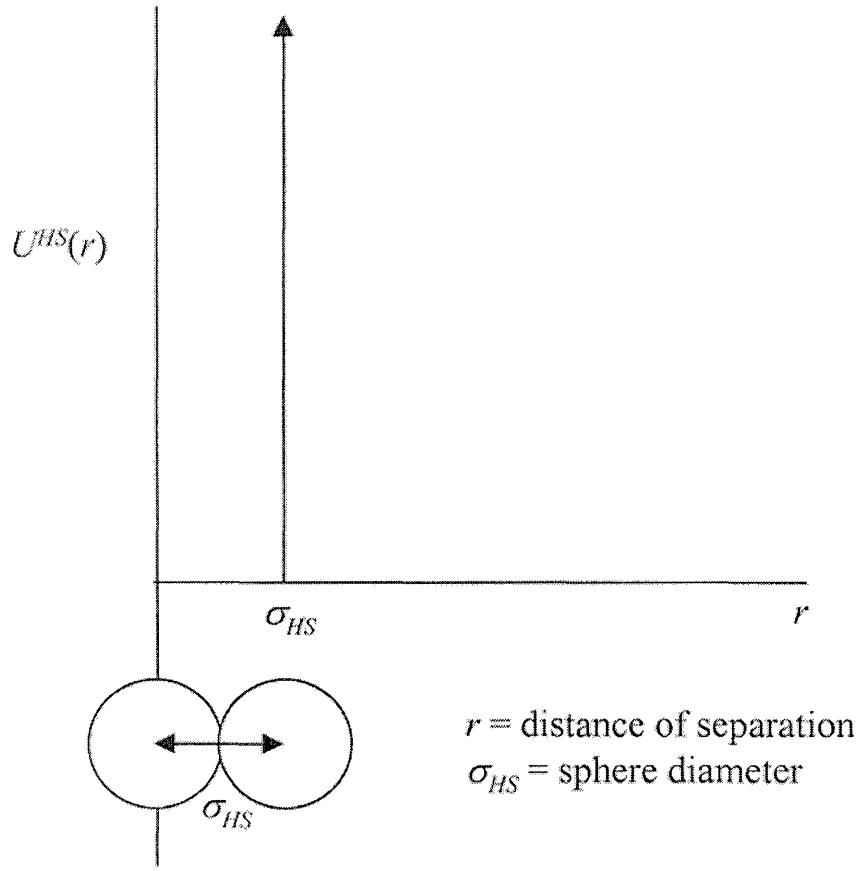

Figure 2-6 Hard sphere interaction.

2.1.2.2 Adhesive Hard Spheres

When these experimental "hard sphere" systems are dispersed in certain solvents and at specific temperatures, the hard sphere interaction deviates from purely repulsive to include a short-ranged attractive contribution. This can be modeled theoretically with the adhesive sphere interaction potential shown in Figure 2-7 and is represented by the following:

$$U^{AS}(r) = \lim_{\sigma' \to \sigma} \begin{cases} \infty & ,r < \sigma' \\ \ln\left[\dfrac{12\tau(\sigma - \sigma')}{\sigma}\right] & ,\sigma' < r < \sigma \\ 0 & ,\sigma < r \end{cases} \qquad [2.16]$$

Several experimental adhesive sphere colloidal systems have been studied as a function of temperature and solvent including the sterically stabilized silica particle dispersions, details of which will be discussed in Section 2.3.1.

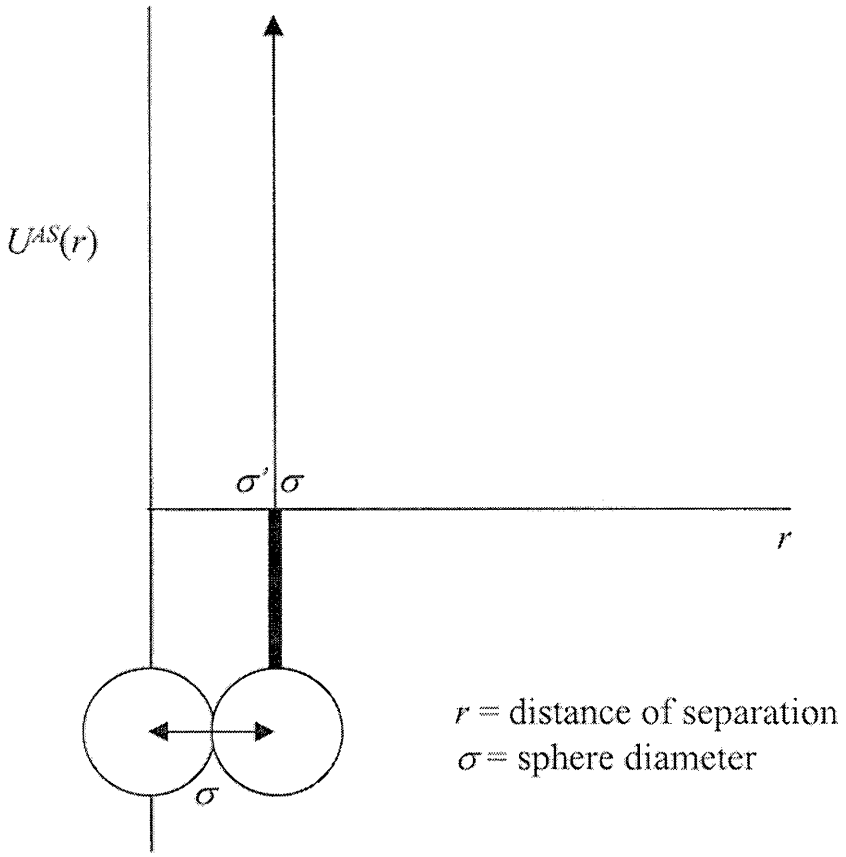

Figure 2-7 Adhesive hard sphere interaction.

2.2 Theoretical Studies of Binary Systems

2.2.1 Simulation Studies

As discussed in [24], the use of computer simulation, such as Monte Carlo (MC) and molecular dynamics (MD) for mixture studies has been performed since the early 1970s. Monte Carlo methods generally include simulations in which energy-weighted probabilities for particle displacement are introduced into the numerical computations. A particle is selected and is displaced from configuration "i" to configuration "j" based on the change in system configurational energy, calculated from the pair potential equation. Molecular dynamics is quite similar to Monte Carlo but uses computers to solve the equations of motion for many spheres simultaneously. Observable macroscopic quantities can be subsequently calculated by time averaging, yielding both dynamic and thermodynamic system properties. Both Monte Carlo and molecular dynamics have been used to study binary mixtures by a number of investigators for both hard sphere and soft sphere systems.

2.2.1.1 Hard Spheres

Solid-fluid coexistence in binary hard sphere mixtures was studied by MC [7] for three mixtures with diameter ratios of 0.95, 0.93, and 0.90. For a diameter ratio, α, of 0.95, the diagram showed spindle-type behavior whereas for α = 0.93 and 0.90 the

diagrams showed an azeotrope. These results correspond well to the MC studies of Kranendonk [25] for α = 0.95 and 0.90. For hard sphere binary mixtures of large size ratio, α = 0.1 [8], MD was used to compute the entropic depletion force felt by large spheres immersed in a fluid of small spheres. Also, by MC, the phase diagram of the binary mixture was determined, showing a spinodal instability in this system.

MC has also been used to study the phase equilibria of symmetric and asymmetric non-additive hard sphere mixtures (NAHS) [26]. This model consists of a mixture of hard spheres whose interactions between unlike particles are characterized by a hard-sphere diameter, $\sigma_{\alpha\nu} = \frac{1}{2}(\sigma_{\alpha\alpha} + \sigma_{\nu\nu})(1+\Delta)$, with Δ being the non-additivity parameter; Δ=0 is for the purely additive system [27]. The equation of state of a NAHS mixture was obtained using MD and it was found that there is a fluid-fluid phase transition at high densities [28]. Both MC and MD were also used to study the thermodynamic stability of the AB (rocksalt) structure for binary mixtures of hard spheres, giving constant pressure and constant volume phase diagrams for binary mixtures of hard spheres with α = 0.414 and 0.45 [29].

In addition to simulation techniques, other methods have been used to study binary mixtures [30]. These include cell theory as introduced by Lennard-Jones and Devonshire to determine bulk properties of molecular fluids. In this approach, an array of particles is replaced by an array of hypothetical cells in which the movement inside is confined. Phase diagrams of binary hard sphere mixtures for α = 0.90 and 0.95 show the

stability of some simple compounds in terms of α, density, and composition [31, 32]. These phase diagrams verify the results from other approaches including the simulations by Kranendonk [24] and Kofke [7], and the density functional theories by Denton [13] and Zeng [33]. From these studies, it can be seen that using simulation techniques, including MC, MD, and cell theory, the phase diagrams for binary hard sphere mixtures can be obtained with good agreement between different techniques.

2.2.1.2 Charged Spheres

Binary charged spheres have been studied by simulation techniques, however most investigations have focused on dynamic behavior and not phase behavior. One MC study performed by Kerley [34] determined an equation of state for soft sphere mixtures and found that at high pressures, large size ratios can lead to phase separation.

To conclude, there have been numerous studies of the phase behavior of binary hard sphere systems using various simulation methods for which there has been good agreement. For binary adhesive systems, there have been no phase studies using simulation techniques and, for binary charged systems, there has been only a few studies via simulation approaches.

2.2.2 Thermodynamic Calculations

2.2.2.1 Hard Spheres

As discussed previously, the hard sphere potential can be used to approximate the interactions in real colloids and for dilute microemulsion systems. It is one of the simplest interactions and a good model for systems of uncharged or sterically stabilized particles. An example of sterically stabilized particles includes those with polymer chains adsorbed on the surface, screening van der Waals attractions and stabilizing the dispersion. Using a theoretical approach, one can determine the structure either analytically or numerically. Analytical solutions are available for both one-component and multicomponent hard–sphere systems, both of which are in agreement with results from computer simulations [3].

To obtain information about structure of colloidal suspensions interacting via a hard sphere potential, one must solve the Ornstein–Zernike (OZ) equation. The OZ equation can be generally expressed as [35]

$$h(r_{12}) = c(r_{12}) + \rho \int c(r_{13})h(r_{23})dr_3 \qquad [2.17]$$

$$h(r_{12}) = g(r_{12}) - 1 \qquad [2.18]$$

where $h(r_{12})$ is the total correlation function and represents the overall effect of molecule 1 on molecule 2 at a distance r_{12}. This equation breaks the total correlation function into

two parts, a direct part $c(r_{12})$, and a second part containing the indirect influence of molecule 1 on molecule 2 via other molecules.

Of particular interest to us is the connection that can be made with experimental light scattering studies. When one multiplies the Fourier transform of $h(r)$ by the density, it is known as the structure factor $S(q)$,

$$S(q) = \rho \int h(r) e^{iq \bullet r} dr$$

an experimentally measurable quantity. [2.19]

To solve the OZ equation, closure relations must be used; examples include the Percus-Yevick, the hypernetted-chain, and the Rogers-Young (RY) closures. For binary mixtures, the Ornstein-Zernike equation can be extended as the following [12, 36]:

$$h_{ij}(r) = c_{ij}(r) + \sum_{k=1}^{2} \rho_k \int dr_k c_{ik}(r_{ik}) h_{jk}(r_{jk}) \qquad [2.20]$$

with the Percus-Yevick (PY) closure [37],

$$c_{ij}(r) = e^{-\beta u_{ij}(r)} \left[\gamma_{ij}(r) + 1 \right] - \gamma_{ij}(r) - 1 \qquad [2.21]$$

the hypernetted-chain (HNC) closure,

$$c_{ij}(r) = e^{-\beta u_{ij}(r) + \gamma_{ij}(r)} - \gamma_{ij}(r) - 1 \qquad [2.22]$$

and the Rogers Young (RY) closure [37],

$$c_{ij}(r) = e^{-\beta u_{ij}(r)} \left[1 + \frac{e^{\gamma_{ij}(r) f_{ij}(r)} - 1}{f_{ij}(r)} \right] - \gamma_{ij}(r) - 1 \qquad [2.23]$$

used, where

ARTHUR LAKES LIBRARY
COLORADO SCHOOL OF MINES
GOLDEN, CO 80401

$$\gamma_{ij}(r) = h_{ij}(r) - c_{ij}(r) \qquad [2.24]$$

and, $f_{ij}(r) = 1 - e^{-\alpha_{ij} r}$. [2.25]

For hard sphere systems, using the PY approximation, the OZ relation for fluid mixtures has been solved for the direct and indirect correlation functions [11, 12] and the radial distribution function [11]. Expressions for the direct correlation function and the radial distribution function for symmetric hard sphere mixtures have also been derived, allowing determination of a virial expansion of pressure up to third power in density [11].

With a self-consistent integral equation connected with Verlet's modified closure, fluid-fluid phase separation in symmetric NAHS mixtures has been studied [27]. The chemical potential of mixtures were determined and the phase diagram constructed. These studies showed that dense binary mixtures of hard spheres phase separated when α <0.2. They were also extended to binary mixtures of hard spheres and Yukawa particles by solving the OZ equation using the RY closure. In these studies, a spinodal line indicating phase separation was observed.

Another analytical approach used for phase diagram prediction is density functional theory. Density functional theory treats the solid free energy as a perturbation of the liquid free energy; the excess free energy of solid is expanded around the excess free energy of a reference liquid [33]. In some studies, it has been assumed that the higher- (than second) order terms in the free energy expansion are small and can be

neglected. An estimation of the third-order term showed that the magnitude was comparable to the second term; therefore, truncation at the second term was not justified [38]. To overcome these problems, the weighted density approximation (WDA) and modified weighted density approximation (MWDA) were developed to account for higher-order terms in the free energy expansion. These theories have been applied to the freezing of single component systems of hard spheres.

In addition to single component calculations, phase diagrams of hard sphere binary mixtures have been determined by DFT [36]. As seen in simulation, it is clear that size ratio has a strong influence on the phase diagram. The freezing behavior of binary hard sphere mixtures with diameter ratio 0.1 has also been investigated by density functional theory. The stability of a sublattice melt (SLM) phase, in which the large spheres are localized on crystal lattice sites and the small ones are fluid-like, was studied [39]. For binary additive hard sphere mixtures, a phase diagram including the SLM has been calculated [40].

Using WDA, the freezing transitions of binary mixtures of hard spheres has been determined and the disordered-fcc crystal structure transition at different hard sphere diameter ratios calculated [13], providing good agreement to the simulation results of [25, 41]. Applications of a DFT of nonuniform fluid mixtures to the fluid-solid transition of simple binary mixtures of hard spheres showed the importance of relative atomic sizes in determining lattice constants. It was also stated that for the small disparities in atomic size, Vegard's law, which is an approximate empirical rule showing a linear relation

between the crystal lattice constant of an alloy and the concentrations of the constituent elements, held along the fluid-solid coexistence curve [42].

The effective liquid free energy model (ELFEM) density functional theory can also be used for the study of nonuniform hard sphere liquids [33]. With this theory, the freezing of a binary hard sphere liquid into a disordered fcc solid has been investigated. Also, by another self-consistent density functional theory, the phase separation of asymmetric binary hard sphere fluids has been studied [43] showing phase separation in bulk binary mixtures with large size ratios of 4:1.

2.2.2.2 Adhesive Hard Spheres

In 1968, Baxter defined the adhesive sphere potential as [44]

$$\frac{U^{AS}(r)}{kT} = \lim_{\sigma' \to \sigma} \begin{cases} \infty & ,r < \sigma' \\ \ln\left[\dfrac{12\tau(\sigma - \sigma')}{\sigma}\right] & ,\sigma' < r < \sigma \\ 0 & ,\sigma < r \end{cases} \qquad [2.26]$$

where σ represents the adhesive hard sphere diameter, τ represents a dimensionless temperature and its inverse is a measure of particle stickiness.

For binary adhesive hard sphere mixtures, the interaction potential can be defined as

$$\frac{U^{AS}_{ij}(r)}{kT} = \lim_{\sigma_{ij} \to \sigma_{ij}} \begin{cases} \infty & ,r < \sigma_{ij}' \\ \ln\left[\dfrac{12\tau_{ij}(\sigma_{ij} - \sigma_{ij}')}{\sigma_{ij}}\right] & ,\sigma_{ij}' < r < \sigma_{ij} \\ 0 & ,\sigma_{ij} < r \end{cases} \qquad [2.27]$$

with

$$\sigma_{ij} = \frac{\sigma_i + \sigma_j}{2} \qquad [2.28]$$

and the diameters of individual species represented by σ_i, i=1,2.

By solving the OZ equation using the PY closure, the liquid-liquid phase diagram for asymmetric (different size) and symmetric (same size) binary mixtures of sticky spheres in the τ and c (concentration) plane has been obtained and the structure factors for Baxter model has been calculated [45]. Using the PY approximation, phase diagrams of binary mixtures of sticky spheres have also been calculated by Jamnik [46]. In these studies, correlation functions between unlike particles showed singularities at particular interparticle distances.

Other studies of the phase behavior of binary mixtures of attractive hard spheres have been performed using a hard-sphere mixture equation of state with a mean field term [47, 48], showing evidence of a closed liquid-liquid immiscibility loop and new azeotropic phenomena.

2.2.2.3 Charged Spheres

In studies of charged hard-sphere mixtures [49], it has been found that the modified hypernetted-chain (MHNCS) closure works well for one-component soft-sphere fluids above and below the freezing point and for binary soft-sphere fluids. Also, by using the MHNCS, equilibrium properties of highly supercooled binary soft-sphere fluids have been evaluated [50]. By solving the OZ equation with the RY closure, structural properties of charged colloidal mixtures have been studied [37]. In addition, the screened Coulomb (Yukawa) charged hard sphere binary fluid has been studied using the generalized mean-spherical approximation (GMSA) and the phase diagram determined [51].

2.3 Experimental Studies of Binary Systems

There have been numerous theoretical studies of the phase behavior of binary hard spheres; however, not much is known for charged mixtures and even less about binary adhesive spheres. To obtain more information on the phase behavior of binary mixtures and to verify results from theory, experimental studies are introduced.

To model binary systems, colloids have been chosen because of experimental advantages discussed in Chapter 1. To represent hard, adhesive, and soft repulsive

spheres, three colloidal systems have generally been used, including colloidal silica, poly(methyl methacrylate) and polystyrene.

2.3.1 Silica

As originally described by Stöber [52] preparation methods allow the synthesis of colloidal silica in a wide range of sizes. In addition to ease of synthesis, octadecyl chains can be easily grafted onto the surface, removing surface charge and short-range repulsive particle interactions. Ions in solution can also be used to make silica behave like hard spheres, screening charge-charge interactions as discussed in Section 2.1.1.1.

This approach has been used to study charged silica particles dispersed in dimethyl formamide (DMF) [16]. Binary mixtures of hard-sphere like silica particles dispersed in DMF with 0.0100M LiCl have been studied at a size ratio of 1:9.3. Through fluorescent labeling, the behavior of each colloid type has been investigated separately using fluorescence recovery after photobleaching (FRAP) [53].

Sterically stabilized silica particle dispersions have been studied as a model of the single-component adhesive hard sphere system. Dispersions of silica particles coated with octadecyl chains in benzene and n-dodecane have been studied by Rouw [54] who found solvent-chain attractive interactions in benzene that became greater when dispersed in n-dodecane. Also in benzene, studies of morphology using small angle neutron scattering (SANS) have found that silica particles behave like adhesive spheres at lower

temperatures and hard spheres at higher temperatures. Turbidity studies have shown the existence of a small interparticle attraction [55] that arises from the interaction between polymer chain segments and solvent. They have been shown to increase as the temperature is lowered [56] leading to the onset of phase separation for sterically stabilized silica particles in toluene as the temperature is decreased [57].

2.3.2 PMMA

To use colloidal poly(methyl methacrylate) (PMMA) as a model system with short-ranged interactions, a layer of poly(12-hydroxy stearic acid) (PHSA) must be grafted onto the particle surface. This minimizes the effect of the van der Waals attraction giving rise to a hard-sphere-like interaction [58].

Binary mixtures of these hard-sphere like sterically stabilized PMMA particles dispersed in a near index matched suspension have been investigated at $\alpha = 0.61$. By varying the volume fraction of both components, light scattering and scanning electron microscopy was used to study the phase behavior [14] where 4 regions are present. When the number fraction of larger component A is greater than 0.43, particles crystallized to form irregularly stacked hexagonal close packed layers containing almost entirely A (I). When the number fraction of A decreased to 0.28, the suspensions remained amorphous and showed glassy behavior (II). At number fractions of A between 0.28 and 0.057, coexistence of crystals of B, the ordered phase AB_{13}, and a binary fluid (III) were

observed. At number fractions of A less than 0.057, irregularly stacked close packed crystals of B (IV) were present. These studies have been extended to binary PMMA particles with a size ratio of 0.31 using small angle neutron and light scattering. Through contrast variation, it was found that the crystalline phase contained mostly larger spheres, A, while the smaller spheres, B, were excluded into a coexisting binary fluid [59]. These studies were later continued for a size ratio of 0.58 using powder light crystallography and electron microscopy. In these studies, both AB_2 and AB_{13} structures were found [60, 61] corresponding well to the results from computer simulations by Eldridge [15].

2.3.3 Polystyrene

Although OH groups are present at the surface of polystyrene colloids, the resulting charge-charge interaction can be screened by dispersing the colloid in salt water making the interaction hard sphere-like [62]. Binary systems of such hard sphere like charged polystyrene colloids have been observed to segregate into large and small regions of different volume fraction and size ratio [63]. Viewed by optical microscopy, the same system has showed evidence of a bulk phase separation into two disordered phases and an ordered phase located on the cell walls [64].

For studies of charged colloidal suspensions, the most commonly used colloidal dispersion is polystyrene. A number of binary mixtures have been investigated by small angle neutron scattering (SANS), including mixtures of charged polystyrene of radius

16.8 and 51.0 nm [20], mixtures of silica and sodium dodecyl sulfate (SDS) micelles [65], and mixtures of polystyrene and silica [37]. By contrast variation, the scattering length density of each component can be matched to the scattering length density of the solvent, allowing the determination of partial structure factors and the colloidal phase diagram.

For mixtures of charged polystyrene particles with radii of 42 and 65 nm [66] and mixtures of charged polystyrene with diameters of 38, 94, and 136 nm [67], studies have been done by static light scattering, allowing the measurement of mixture structure factors. Results from these studies were in good agreement with the results from thermodynamic calculations.

Mixtures of polystyrene and mixtures of silica particles have also been investigated by close-up photography. By varying the volume fraction of both components, liquid and crystal states have observed and the phase diagram determined [68].

In summary, experimental studies of binary system phase behavior have been conducted for hard and charged sphere mixtures. However, experimental studies have not yet to be conducted on the systems where an attractive interaction is present.

CHAPTER 3

CORE-SHELL SYSTEMS

3.1 Motivation

In recent years, colloidal systems have proven to be useful thermodynamic models of molecular systems with simple interactions. Colloids have been chosen to represent these simple systems because they can be synthesized in the mesoscale range from nanometers to microns, and their interactions can be easily tuned by changing solvent or temperature. One additional advantage in using such systems is that they can be directly manipulated using optical trapping techniques [69]. In this approach, the extent of the manipulating or trapping force depends on the mismatch of particle and solvent refractive indices. This required difference in refractive index between particles and solvent, however, leads to a strong interparticle van der Waals attraction that may not be desirable in a given study. One approach to uncoupling these interactions from the trapping force is to use a core-shell system. By index matching the shell with solvent, interparticle van der Waals interactions can be minimized, yet the optical trapping approach can still be used to trap particles because of the index of refraction difference between the solvent and core.

In recent decades, a strong desire to improve the properties of ceramic materials has brought great interest to the sol-gel synthesis process. One of the major advantages of this process is that mixing of multicomponent systems on the nanoscale [70] can be achieved. One approach to such intimate mixing is the deposition of uniform layers of one material on a solid of different composition, effectively achieving a core-shell synthesis. The primary objective of such an approach is to improve the properties of the core [71] including chemical, magnetic, and optical properties. This often has the effect of improving the particle dispersability in solvents or in a matrix phase within a composite [72]. Also in the case of precious materials, it can be economical to coat expensive reactants on an inexpensive core [71]. Such core-shell processes are certainly more complex than traditional syntheses, however, great interest has arisen in them due to their many applications.

As discussed by Matijević [73], a dispersion of two components can be prepared by precipitating a new phase in the presence of existing particles, resulting in situations where either new particles form, particles heterocoagulate, or a layer of the new phase can form on the existing particles. The parameters that control this process are the concentration of the precipitating species, the number of preformed particles present, the particle surface charge, and in some cases, pH and temperature also become important factors.

Core-shell synthesis was patented by Iler [74], where particles with a silica shell and a core of different materials, including clays, talc, alumina, zinc sulfide, and titania

was discussed. To examine the surface properties of such core-shell particles, Furlong [75] investigated the precipitation of silica on the surface of titanium dioxide by measuring the solubility using electrophoresis. Also, there have been several studies using a variety of techniques to study the chemical and physical properties of coated titanium dioxide surfaces. These include electron microscopy [76] and gas adsorption [76, 77]. These studies have found that spherical titanium dioxide cores can be prepared by hydrolysis of titanium (IV) ethoxide and dehydration to obtain TiO_2 particles [78, 79]. Other methods to prepare titanium dioxide particles have been described by Visca [80] and Look and Zukoski [81].

To directly manipulate colloidal systems, optical trapping techniques have been recently developed and are based on the use of radiation pressure to manipulate an individual colloidal particle [82]. In this, a single focused laser beam is used to trap a small colloidal particle in 3-dimensions and to prevent it from settling against gravity or diffusing in its solvent. For stable trapping, the trap must overcome the scattering and absorption forces pointing down and destabilizing the trap [83]. This works for large Mie particles, and Svoboda and Block [83] have demonstrated that small Rayleigh particles; $\lambda >> a$, can also be trapped in 3 dimensions. Instead of trapping a few particles, however, multiple particles can be simultaneously trapped by using multiple laser beams or by using a single scanning laser beam as shown by Mio and Marr [84]. With this technique, one can directly manipulate ensembles of colloidal particles.

Because the extent of the trapping force depends on the mismatch between the particles and solvent, index matching between colloid and solvent will minimize the van der Waals attraction but will not allow optical trapping. A core-shell system could make this technique usable if it were synthesized with materials of very different indices of refraction. This chapter describes the synthesis of silica-coated titania particles, lowering significantly the van der Waals interactions among particles in silica-index matching solvents and illustrating that the resulting colloids can be manipulated using optical trapping techniques.

3.2 Design

To estimate the required thickness of silica shell needed to minimize the van der Waals attraction between spheres, we need a means of predicting dispersion forces between core-shell systems. The Hamaker theory [18] allows one to calculate the overall van der Waals potential between two colloids separated at a distance r by summing up individual molecular contributions via

$$U^{vdW}(r) = \frac{-1}{\pi} \int_{V_1} \int_{V_2} \frac{A}{r'^6} d\mathbf{r}_1 d\mathbf{r}_2 \qquad [3.1]$$

where A is the Hamaker constant and $r' = |\mathbf{r}_2 - \mathbf{r}_1|$. This expression is convenient because it reduces to relatively simple analytic forms for simple geometries such as identical interacting spheres [18]. Integration of this equation for a core-shell system, however, is

significantly more complicated because the Hamaker constant is not constant within the volume integrals. Assuming pairwise additivity though, one can break up the integral for core-shell titania/silica systems into the sum of contributions from solid spherical particles as

$$U^{vdW}(r) = -\frac{1}{\pi^2}\begin{bmatrix} \int_{V_{1c}^T}\int_{V_{2c}^T}\frac{A_{TT}}{r'^6}d\mathbf{r}_{1c}d\mathbf{r}_{2c} + 2\int_{V_{1c}^T}\int_{V_2^T}\frac{A_{ST}}{r'^6}d\mathbf{r}_{1c}d\mathbf{r}_2 \\ -2\int_{V_{1c}^S}\int_{V_{2c}^T}\frac{A_{ST}}{r'^6}d\mathbf{r}_{1c}d\mathbf{r}_{2c} + \int_{V_{1c}^S}\int_{V_{2c}^S}\frac{A_{SS}}{r'^6}d\mathbf{r}_1 d\mathbf{r}_2 \\ -2\int_{V_{1c}^S}\int_{V_2^S}\frac{A_{SS}}{r'^6}d\mathbf{r}_{1c}d\mathbf{r}_2 + 2\int_{V_{1c}^S}\int_{V_{2c}^S}\frac{A_{SS}}{r'^6}d\mathbf{r}_{1c}d\mathbf{r}_{2c} \end{bmatrix} \quad [3.2]$$

where S = silica, T = titania, and the subscript c indicates the core. This calculation is illustrated graphically in Figure 3-1.

It is convenient to break up the integral in this fashion because expressions for van der Waals interactions between non-identical solid spheres are available. Mahanty & Ninham [18] have modeled the dispersion interaction with the following:

$$U^{vdW}(r) = -A_{eff}(r-2a)H\left(\frac{r}{a}\right) \quad [3.3]$$

where A_{eff} = effective Hamaker constant. For partially retarded systems

$$A_{eff} \approx \frac{3}{4}kT\left(\frac{\bar{\varepsilon}(0)-\varepsilon(0)}{\bar{\varepsilon}(0)+\varepsilon(0)}\right)^2 + \frac{3h\omega}{32\sqrt{2}\pi}\frac{\left(\bar{n}_0^2-n_0^2\right)^2}{\left(\bar{n}_0^2+n_0^2\right)^{3/2}}\left[1+\left(\frac{\pi H'}{4\sqrt{2}}\right)^{3/2}\right]^{-2/3} \quad [3.4]$$

with $$H' = n_0\left(\bar{n}_0^2+n_0^2\right)^{1/2}\frac{(r-2a)\omega}{c} \quad [3.5]$$

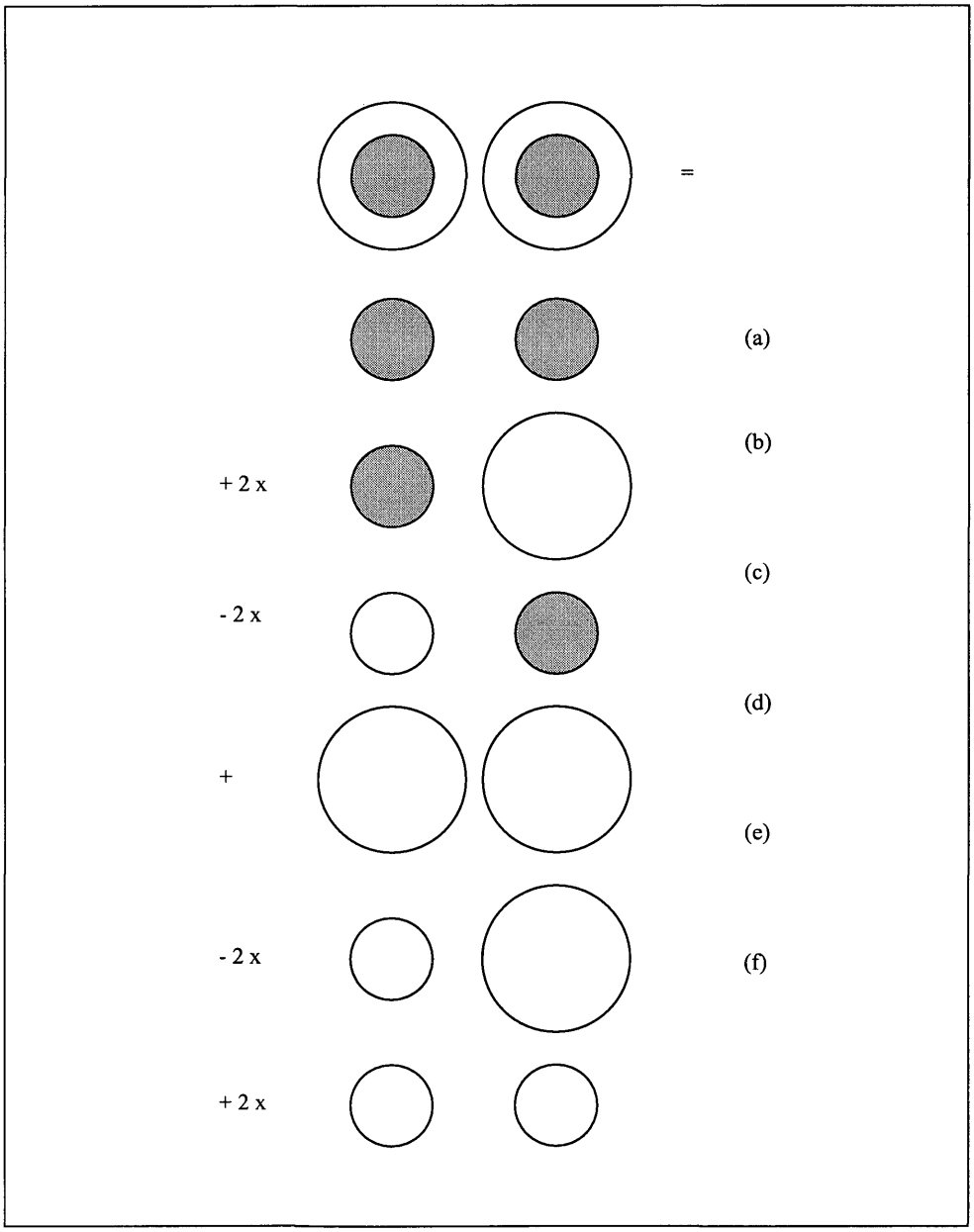

Figure 3-1 Overall core-shell particles interactions (◯ , silica; ◍ , titania), (a) = core-core interaction, (b)+(c) = core-shell interaction, and (d)+(e)+(f) = shell-shell interaction.

where $\bar{\varepsilon}(0)$ and $\varepsilon(0)$ represent the dielectric constant of sphere and medium, $\bar{n}_0$ and n_0 are the index of refraction of the sphere and medium, h is Planck's constant, and ω is the primary absorption frequency of the colloid. For two spherical particles with radii a_1 and a_2, $H\left(\frac{r}{a}\right)$ becomes

$$H\left(\frac{r}{a}\right)=\left(\frac{2a_1a_2}{r^2-(a_1+a_2)^2}+\frac{2a_1a_2}{r^2-(a_1-a_2)^2}+\ln\frac{r^2-(a_1+a_2)^2}{r^2-(a_1-a_2)^2}\right)/6 \qquad [3.6]$$

By now combining values of A_{TT} and A_{SS} from Equation 3.4 and an estimate for A_{ST} from Hiemenz [17]

$$A_{ST}=\sqrt{A_{SS}A_{TT}} \qquad [3.7]$$

one can predict the overall van der Waals interaction between core-shell colloids. These can be combined into three separate terms representing core-core, core-shell, and shell-shell interactions between colloids. Figure 3-2 illustrates the relative significance of these terms, where, at small shell thicknesses, the core-core interaction dominates but as the shell thickness increases, the shell-shell interaction becomes much more important.

In order to prevent particle contact (and agglomeration), short polymer chains are often grafted on the colloid surface. The total interaction between two such particles therefore becomes

$$U^{total}(r)=U^{vdW}(r)+U^{poly}(r). \qquad [3.8]$$

Between colloidal particles with grafted polymer chains, the interaction potential can be modeled as [21]

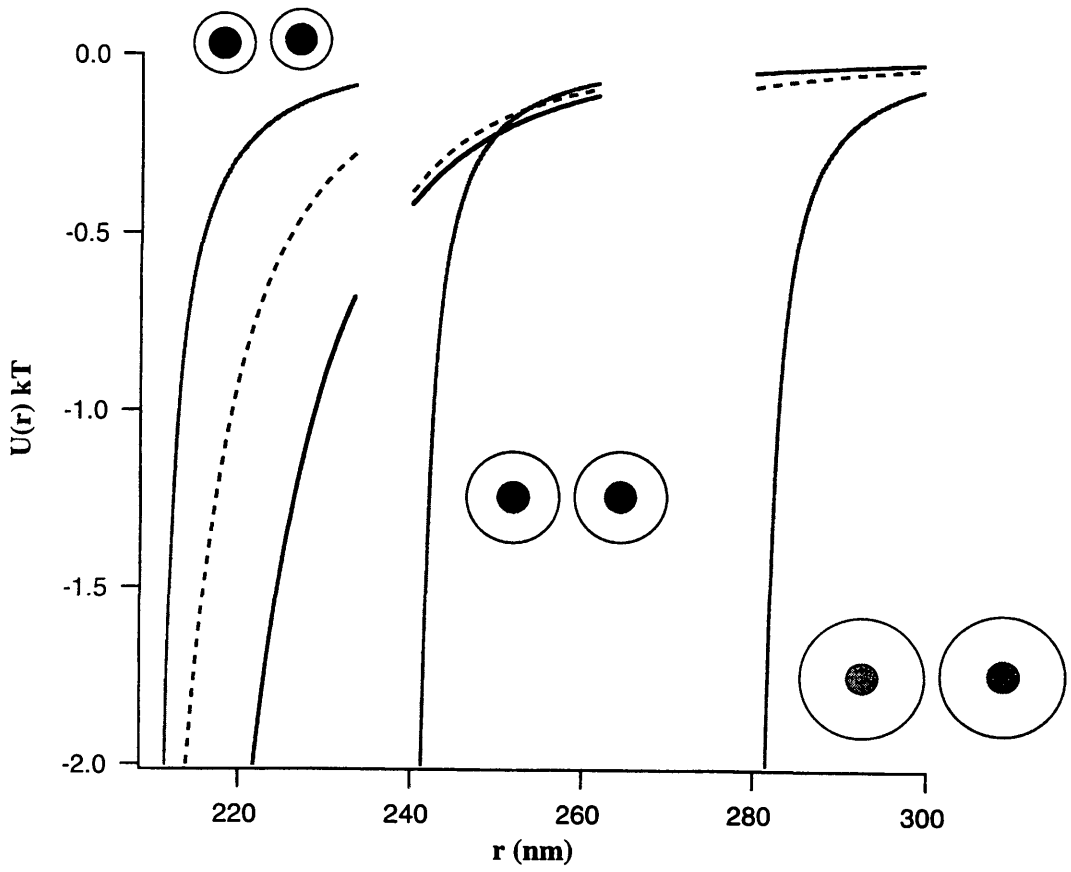

Figure 3-2 Predicted contributions to the vdW interaction between core-shell titania/silica particles at separation r for a core radius of 100 nm. (a) $\delta = 5$ nm, (b) $\delta = 20$ nm, and (c) $\delta = 40$ nm.

(——— core-core interaction, - - - - - - core-shell interaction, and ——— shell-shell interaction) The illustrations of shell thicknesses are exaggerated for clarity.

$$U^{poly}(r)=\begin{cases}\infty & ,r<2a \\ U_0\left[-\ln(y)-\frac{9}{5}(1-y)+\frac{1}{3}(1-y^3)-\frac{1}{30}(1-y^6)\right] & ,2a<r<2(a+L) \\ 0 & ,r>2(a+L)\end{cases} \qquad [3.9]$$

where

$$y=\frac{r-2a}{2L} \qquad [3.10]$$

and

$$U_0=\left(\frac{\pi^3 L\sigma_p}{12N_p l^2}k_B T\right)aL^2. \qquad [3.11]$$

Here, a is an overall core-shell particle radius, L is the polymer layer thickness, N_p is the number of segments in the polymer chain, l is the length of a segment, and σ_p is the surface grafting density. By estimating an octadecyl chain thickness of 2.29 nm, segment length of 0.127 nm, and surface coverage of 0.2 nm^2/chain [85], a U_o on the order of 10^{-16} J is calculated.

Prediction of the interaction potential due to polymer grafting shows a strong repulsion at small separations that becomes negligible at twice the polymer layer thickness. The van der Waals interaction however is strongly attractive at small separations and only gradually decreases in magnitude as the particle separation increases. Combination of the surface polymer repulsion and the van der Waals attraction results in a net attractive well at small separations. Determination of the well depth at a variety of shell thicknesses shows that as the thickness of the silica shell increases, the

well depth decreases; however, at large shell thicknesses the well depth can actually increase as the shell thickness increases. From this, and somewhat surprisingly, it is clear that an optimum shell thickness exists for a given titania core size. Figure 3-3 shows the well depth vs. γ, the ratio of silica shell thickness (δ) to titania core radius (a), where the optimum shell thickness (δ^*) is also plotted. Figure 3-3 guides our core-shell colloidal particle synthesis; for example, a titania core of radius 250 nm should have a 70 nm shell to minimize the attractive well depth.

To lower the magnitude of the van der Waals interaction, core-shell particles were dispersed in index matching solvents. After completing the index matching of silica shell and solvent, the index mismatch between titania core and solvent provides sufficient trapping force for optical trapping to be useful at moderate laser powers. To test the index matching between the silica and solvents, silica particles were prepared via the methods of Stöber [52], van Helden [85], and Al-Naafa [86] and were added to the system of silica-coated titania particles.

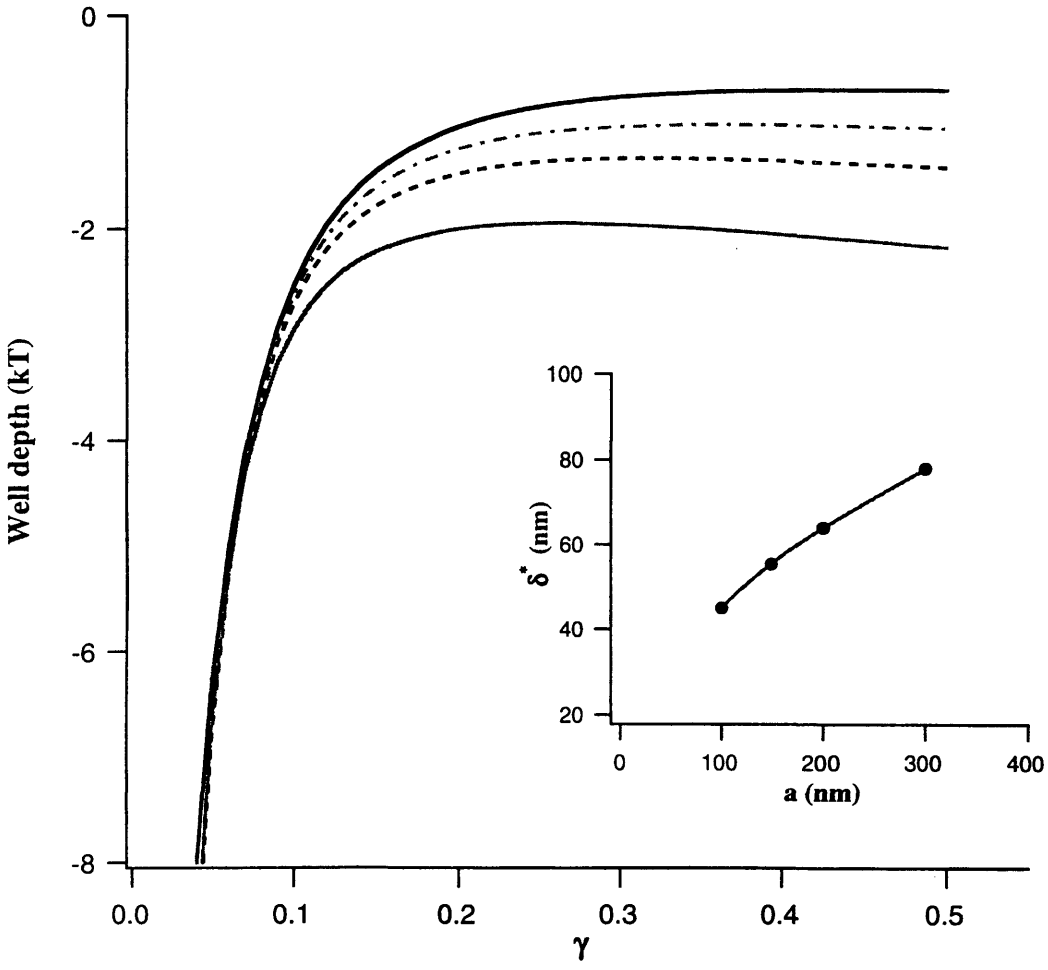

Figure 3-3 Well depth vs. silica shell thickness for various titania core sizes. $\gamma = \delta/a$ (—— $a = 100$nm, - · - · - $a = 150$ nm, - - - - - $a = 200$ nm, and —— $a = 300$ nm). The inset shows the optimum silica shell thickness (δ^*) vs. titania core radius (a).

3.3 Synthesis

To obtain core-shell titania/silica particles, the preparation was divided into two steps, the preparation of titania cores and the coating of the core with silica. In addition, to confirm that the silica shell is completely index-matched, pure silica particles were added to the dispersion and had to be synthesized. After obtaining silica and silica coated titania particles, and to prevent aggregation, polymer chains were grafted onto the surface by an esterification reaction.

3.3.1 Silica

Stable dispersions of colloidal silica can be produced by the chemical reaction of tetra-esters of silicic acid (tetra-alkyl silicates) in water catalyzed by acidic or basic solutions [87]. Aelion [88] studied the hydrolysis of a specific silicate, tetraethyl orthosilicate (TEOS), and showed that the overall reaction occurs in two steps: hydrolysis of ester to silicic acid and dehydration of silicic acid to form amorphous silica. Matsoukas and Gulari [89, 90] and Bogush and Zukoski [91, 92] have also investigated the mechanisms of silica particle formation and growth.

Methods for preparing monodisperse silica sols covering a large size range, 50 to 2000 nm in diameter, have been provided by Stöber [52]. Various other size ranges have been successfully synthesized monodisperse by van Helden [85] and between 10 to 500

nm by van Blaaderen [93]. In his synthesis, Stöber [52] found that ethanol is a suitable solvent when ammonium hydroxide is used as catalyst. The resulting reaction between tetra-alkyl silicates and water under controlled conditions produces silica particles with a narrow size distribution. Due to the reliability of this approach, Stöber's method was used in our experiments.

In the synthesis, there are three important factors in obtaining the highest uniformity and sphericity [86]:

1. The TEOS must be extremely pure.
2. The well-stirred condition must be maintained.
3. Only clean glassware should be used for the same reaction every time.

After synthesizing silica particles via this process, transmission electron microscopy (TEM) was used to characterize the silica colloid size and distribution.

At the surface of a silica particle, at this stage in the synthesis, hydroxyl groups are present. At moderate pH, these anions provide a long-range electrostatic repulsive interaction between individual particles. In order to neutralize the surface charge for studies of short-ranged interactions, these charges can be removed by surface esterification [85, 86, 94, 95, 96].

3.3.2 Silica-Coated Titania

In order to optically manipulate colloids, an index of refraction difference between the solvent and colloid must exist. To manipulate a silica sol in an index-matching solvent, these silica particles must have a core of different refractive index. To prepare core-shell particles, titania was chosen to use as a core because it can be synthesized via similar chemistry as silica and has a higher refractive index ($n = 2.2$) than silica ($n = 1.4$). With this high index of refraction, titania cannot be matched with typical solvents and can be trapped by the optical methods mentioned previously.

From the studies of Jean and Ring [79], titanium oxide particles can be produced via the following reaction:

$$Ti(OC_2H_5)_4 + 4H_2O \leftrightarrow Ti(OH)_4 + 4C_2H_5OH$$

$$Ti(OH)_4 \leftrightarrow TiO_2 .xH_2O \text{ (solid)} + (2\text{-}x)H_2O$$

where ethanol is the solvent and ammonium hydroxide is used as a catalyst.

The general procedure for preparing titania particles is similar to that for silica but replacing TEOS with TEOT or titanium (IV) tetraethoxide for the starting material. The ratios of TEOT, ammonium hydroxide, and absolute ethanol used are presented in Table 3-1. After the reaction was complete, titania particles suspended in ethanol were obtained.

To synthesize the core-shell system, the suspension of titania in ethanol was centrifuged and decanted in order to remove ethanol and then partly redispersed in water.

The coating procedure followed Iler [97], where the suspension of titania in water was first adjusted to pH 10 using sodium hydroxide. The slurry was heated to 95 °C, and then a sodium silicate solution (containing 4% SiO_2 and 1.2% Na_2O) and 1.57% sulfuric acid were added simultaneously but separately during vigorous agitation. The addition continued until the pH approached 8.7. The suspension was then filtered, washed, and the pH adjusted to approximately 6.5 using sulfuric acid. Finally, the suspension was filtered, washed, and dried. TEM was subsequently used to characterize the size of the resulting core-shell particles.

Table 3-1 Silica (S) and titania (T) particle synthesis. Ts2 represents T2 after silica deposition. (* from TEM, ** technical grade ethanol used).

	Volume Ratio				**Diameter (nm)**
	Absolute ethanol	**98% TEOS**	**Tech. TEOT**	**29.4%NH_4OH**	
S_1	26.2**	1.0		1.8	143.8 ± 15.6*
S_2	23.2**	1.0		2.0	356.9 ± 15.2*
T_1	20.0		0.5	~0.3	~300
T_2	20.0		1.0	~0.2	565 ± 80*
T_{s2}					687±220*

3.3.3 Esterification

The esterification of silica and silica-coated titania particles takes place via the following reaction:

$$SiOH + ROH \leftrightarrow SiOR + H_2O \quad (R = \text{Octadecyl}).$$

In our experiments, the procedure followed that of Al-Naafa and Selim [86]. To remove excess octadecanol, the suspension was typically centrifuged at 4,000 rpm with warm (40°C) cyclohexane to separate the esterified particles from the excess octadecanol and the supernatant discarded. After the particles were obtained, TEM was used to characterize the resulting esterified colloids.

3.4 Characterization

3.4.1 Transmission Electron Microscopy

For characterization, the alcosols were dispersed at very dilute concentration and examined via transmission electron microscopy (TEM). A copper TEM grid covered with a carbon film was placed on a flat surface and a drop of alcosol placed on the grid and allowed to dry overnight. Electron micrographs of the particles on the grid were obtained with a Philips EM 400 transmission electron microscope. The magnification was calibrated by means of a germanium shadowed carbon replica of 54864 lines/inch. Both charged and esterified silica particles of diameters approximately 130 nm (type S_1)

and 260 nm (type S_2) were prepared and micrographs of charged silica are shown in Figure 3-4a and of esterified silica in Figure 3-4b. Micrographs of titania core of diameter approximately 550 nm (type T_2) and silica-coated titania (type T_{s2}) are shown in Figure 3-5.

3.4.2 Energy Dispersive Spectroscopy

Due to the high variation of particle-size obtained using TEM, energy dispersive spectroscopy (EDS) was used to confirm that silica layers indeed coated the titania core. In this technique [98], a 1000 nm x 1000 nm area of the sample is bombarded with electrons, which excites the outer shell of each atom causing the emission of x-rays. A beryllium detector measures the x-ray pulse and a histogram of all energies is collected corresponding to the elements present within the sample. Assuming total penetration, overall sample composition can be estimated from a measurement of the relative peak intensity of each element.

To prepare a sample, the alcosol of silica-coated titania particles was diluted and dropped onto a copper TEM grid covered with a carbon film and left to dry. Particle-composition ratios between SiO_2 and TiO_2 were estimated from the intensity of the peaks corresponding to Si and Ti. The silica shell thickness could be estimated from the particle size of the titania core. The silica shell thickness determined from this procedure is ~80 nm for a titania core diameter of ~565nm.

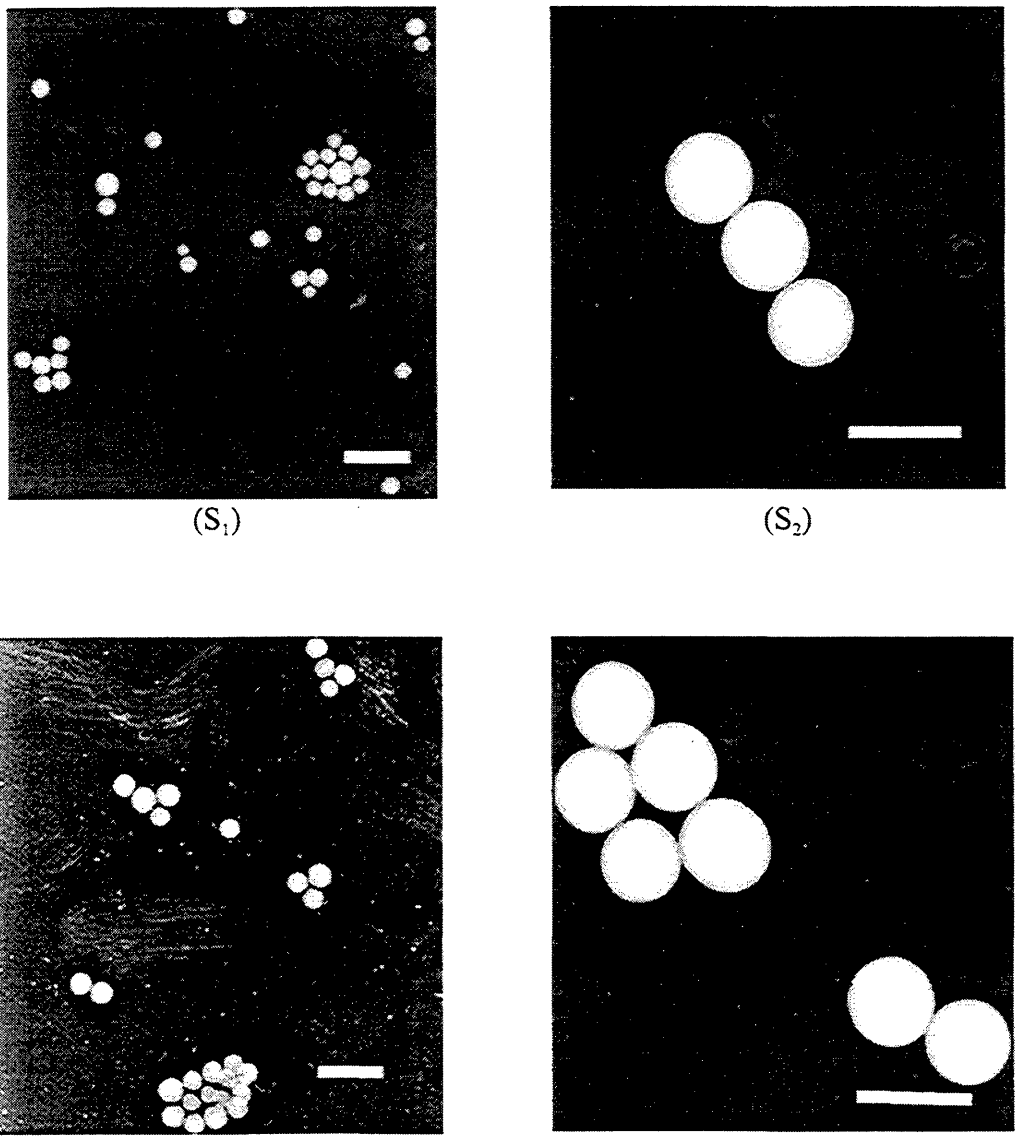

Figure 3-4 TEM micrographs of silica particles type S_1 and S_2. (a) before esterification, and (b) after esterification. The scale bar represents 0.5 μm.

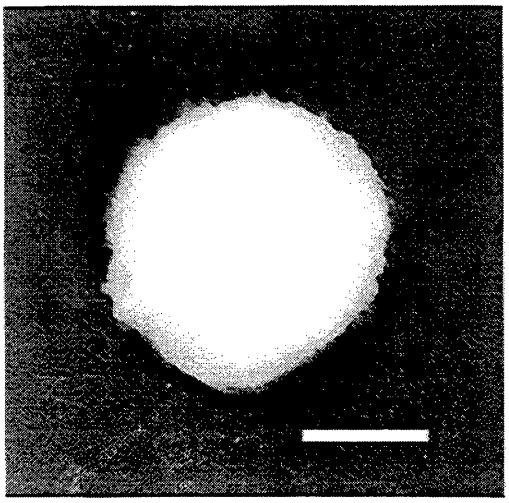

(a)

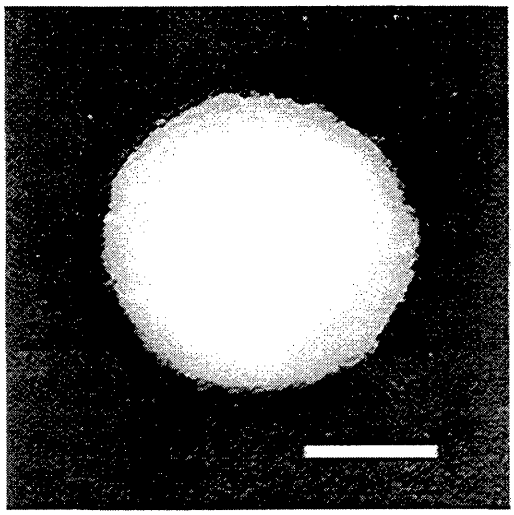

(b)

Figure 3-5 TEM micrographs of (a) titania core T_2 and (b) silica-coated titania particle T_{s2}. The scale bar represents 0.25 μm.

3.5 Optical Trapping

3.5.1 Experiments

Trapping was performed using a Nd:YAG laser of 532 nm at a power of 0.2 W. The beam was Gaussian in shape and vertically polarized with an initial diameter of 2.5 mm but focused down to a spot size of 1 μm for trapping. To have various optical trapping patterns, the beam was scanned using a piezoelectric mirror at a frequency of 300 Hz. Experimental details are presented by Mio and Marr [84].

For sample preparation, a solvent mixture of toluene and propanol was chosen to index match. The solution was transferred into a thin cell made of a cover slip adhered to a microslide using epoxy. The epoxy was applied such that a small space on opposite sides of the slide remained for a solution entrance and exit. After the solution was introduced into the thin cell, wax was immediately used to plug the holes to prevent evaporation of the solvent.

3.5.2 Results

In our colloid synthesis, it was possible to obtain silica particles more monodisperse than titania particles. Due to the polydispersity of the titania cores, the estimation of silica shell thickness was difficult and was only determined approximately as 80 nm for the titania core diameter of ~565 nm. To synthesize monodisperse core-

shell colloids we must lower the core polydispersity which we may be able to achieve by improving the quality of our reagents or through physical separation methods. In addition, we believe that addition of the silica shell may tend to lower the overall polydispersity as seen in the pure silica synthesis.

Optical trapping was confirmed by moving the stage or changing the position of the scanning trap and monitoring the resulting colloid translation. A picture of three core-shell colloids trapped in a triangular pattern is shown in Figure 3-6. In order to verify that the silica shell was indeed index matched, mixtures of silica-coated titania and pure silica particles in the silica index-matching solvents were prepared. In such index-matching solvents the core-shell particles could clearly be seen; however, the esterified silica particles were only faintly visible in index-matched fluids and could not be trapped.

In mixed systems of silica and silica-coated titania particles in index-matching solvents, the trapping of the silica-coated titania was certainly possible but needed to be performed quickly before particles settled and adhered to the glass slide. Settling of the dense core-shell particles was perhaps the greatest experimental difficulty encountered in these experiments. Because a solvent of equivalent density is not available, future work should involve the synthesis of smaller colloids and the use of more viscous solvents to reduce settling velocities.

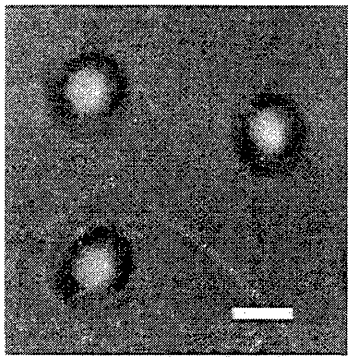

Figure 3-6 Core-shell titania/silica particles in shell index-matching solvent trapped in a triangular pattern and viewed under an optical microscope at high magnification. The scale bar represents 0.5 μm.

CHAPTER 4

CONTRAST VARIATION SYSTEMS

4.1 Motivation

There are several reasons for choosing colloids to represent the model systems discussed in Section 1-1. Since colloidal particles have a size range of nanometers to microns, they are particularly suited for investigation by scattering techniques. Scattering provides several advantages over other characterization approaches; for example, sample preparation is relatively simple and does not alter sample morphology. In addition, there are various kinds of scattering techniques available including x-ray, neutron, and light scattering that can be used for various length scale studies. In our systems, the colloids are between 100-1000nm; therefore, scattering using light of wavelength in the visible range is appropriate.

To investigate colloidal systems using light scattering, there must be a difference in the index of refraction between colloids and their solvent. This is true for both single component and binary systems, the index of refraction of both colloidal types must be different from the solvent index in order to scatter light. In addition, in order for a scattering approach to distinguish between two different kinds of colloids, there must be a difference in index of refraction between each.

Silicon is the most abundant metal in the earth's crust. For this reason and not surprisingly, there is evidence showing the formation of silica gels and sols by hydrolysis and condensation in many natural systems [99]. Since colloidal silica is also used in various fields such as catalysis, metallurgy, electronics, glasses, ceramics, optics, and industrial chromatography [100], the synthesis of silica in crystalline or amorphous states was introduced in 1941 [87]. For synthetic preparation, hydrolysis of metal alkoxides has been widely used in the preparation of colloidal metal (hydrous) oxides, and the same procedure can be employed for the syntheses of mixed metal oxides [101].

In order to study binary mixtures via light scattering, two different kinds of colloids having different indices of refraction must be used. Our approach is to develop a system where one component is colloidal silica, chosen due to its availability in a large size range and the ability to prepare it with good uniformity. Since the other component in our mixture must have a slightly different index of refraction, we propose the use of a silica based oxide due to its unique ability to readily form multicomponent silicates.

The syntheses of multicomponent silicates have been discussed by Brinker [99], where the preparation of SiO_2-Al_2O_3, SiO_2-B_2O_3, and SiO_2-TiO_2 is briefly presented. The preparation of aluminosilicates is of great interest to us since it has been investigated for the synthesis of mullite ($3Al_2O_3$-$2SiO_2$). Although there have been relatively few fundamental investigations on the hydrolysis and condensation of such materials, there has been some study of the synthesis of Al_2O_3-SiO_2 gels by hydrolysis of aluminosilicate ester at room temperature in acidic conditions [102]. Using these studies as a basis, we

will modify the preparation in order to form aluminosilicate sols, details of which are discussed in the following section. Because of a different density and the presence of Al, aluminosilicate particles are predicted to have a refractive index slightly higher than silica.

By now dispersing these two colloidal types in solvent mixtures, the system contrast can be varied by changing the solvent ratio. When the solvent mixture has a refractive index close to silica, silica particles will not be visible and only aluminosilicate particles will scatter. When the solvent is at a mixture ratio now matched for aluminosilicate, only pure silica particles will scatter. This contrast variation method will allow the investigation of each component individually in a binary mixture.

4.2 Synthesis

As discussed above, in binary mixture studies via light scattering, the other colloidal component must have a refractive index slightly different than silica. Since the refractive indices of silica and alumina are approximately 1.4 and 1.6, respectively, a mixture of the two should have an index of refraction within this range. Therefore, we choose aluminosilicate particles and synthesize these via a procedure that is quite similar to the colloidal silica. Aluminosilicate preparation is discussed in detail in the following section including the grafting of polymer chains onto the surface by esterification to prevent aggregation.

4.2.1 Silica

Preparation of silica sols follows the procedure outlined in Section 3.3.1.

4.2.2 Aluminosilicate

There have been studies involving the preparation of silica-alumina particles [101, 102, 103] including aluminosilicate gels [103]. By modifying the gel synthesis procedures, we will prepare aluminosilicate sols. Aluminosilcate particles can be prepared by the reaction of aluminosilicate ester, *di-s*-butoaluminoxytriethoxysilane, in water, catalyzed by ammonium hydroxide. Since the ester is immiscible in water, isopropanol must be present to act as a mutual solvent. Reactant ratios are shown in Table 4-1.

Table 4-1 Aluminosilicate particle synthesis.

Volume Ratio		
Isopropanol (ml)	*di-s*-butoaluminoxytriethoxysilane (ml)	NH_4OH (ml)
1	33.2	2.2

Before a reaction is started, isopropanol is first transferred into a round–bottom flask and stirred vigorously. The ester is then transferred into the flask and, after the ester is completely dissolved in the alcohol, ammonium hydroxide is transferred into the solution. At this point, the reaction begins. As the reaction proceeds, the solution color gradually changes from clear, to bluish, and then to white. The solution is stirred for at least 24 hours. Particles are removed from the suspension by first centrifuging at 10,000 rpm for 15 minutes, and then redispersing in absolute ethanol. This process is repeated until the ammonium hydroxide and isopropanol have been removed from the particles suspended in absolute ethanol.

The overall reaction occurs in two steps:

Step 1: Hydrolysis of the ester to acid:

$$(C_4H_7O)_2Al-O-Si(OC_2H_5)_3 + H_2O \rightarrow (C_4H_7O)_{2-x}(HO)_xAl-O-Si(OC_2H_5)_{3-y}(OH)_y + xC_4H_7OH + yC_2H_5OH$$

$x = 0,...,2$ and $y = 0,...,3$

Step 2: Dehydration of the acid to form amorphous aluminosilicate:

$$(C_4H_7O)_{2-x}(HO)_xAl-O-Si(OC_2H_5)_{3-y}(OH)_y \rightarrow (C_4H_7O)_{2-x}O_xAl-O-Si(OC_2H_5)_{3-y}O_y + \left(\frac{x+y}{2}\right)H_2O$$

$x = 0,...,2$ and $y = 0,...,3$

4.2.3 Esterification

The esterification of silica and aluminosilicate particles is subsequently performed via the following surface reactions:

$$SiOH + ROH \leftrightarrow SiOR + H_2O$$

and

$$AlOH + ROH \leftrightarrow AlOR + H_2O$$

where, R = Octadecyl. In our experiments, the procedure followed that of Al-Naafa and Selim [86], as described in Section 3.3.4. To remove excess octadecanol, the suspension was typically centrifuged at 4,000 rpm with warm (40°C) cyclohexane to separate the esterified particles from the excess octadecanol, and the supernatant discarded. After the particles were obtained, TEM and DLS were used to characterize the resulting esterified particles.

4.3 Characterization

4.3.1 Transmission Electron Microscopy

For characterization, the alcosols were dispersed at very dilute concentration and examined via transmission electron microscopy (TEM). Sample preparation details are described in Section 3.4.1. Esterified silica particles of approximately 360 nm diameter are shown in the micrograph, Figure 4-1. For aluminosilicate particles, some sample

preparation difficulties were present; when a drop of suspension was placed on a copper grid and allowed to dry overnight, it was found that aggregation commonly occurred. Small grid areas however, did provide good images for the particle size measurement. A micrograph of aluminosilicate particles (before esterification) of approximately 240 nm diameter is shown in Figure 4-2. Measurement results are given in Table 4-2.

4.3.2 Dynamic Light Scattering/Zeta Potential Measurement

Due to the sample preparation difficulties present with aluminosilicate particles, dynamic light scattering (DLS) was also introduced for particle size measurements. Dilute suspensions of silica and aluminosilicate particles in water were prepared and dispersed using an ultrasonicator. Subsequently, the suspension was transferred into a polystyrene cell and placed in the sample holder [ZetaPlus Particle Sizing/Zeta Potential, Brookhaven]. Measurement was performed at an angle of 90° and the results are given in Table 4-2.

The zeta potential of silica and aluminosilcate particles both before and after esterification was also measured. To do so, both suspensions in water were transferred into the polystyrene cells and the gold cathode placed into solution. The measured zeta potential and conductance are provided in Table 4-2.

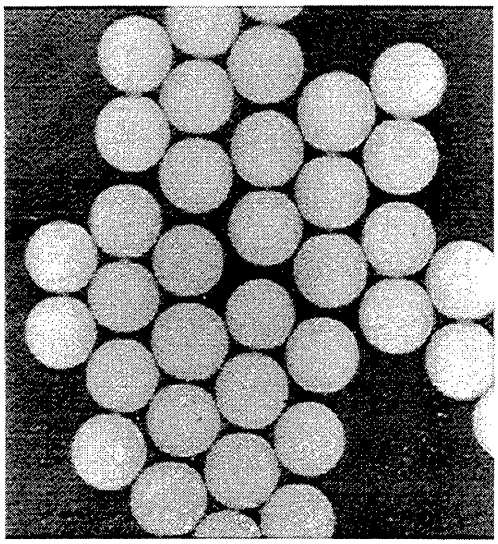

Figure 4-1 A TEM micrograph of esterified silica particles (type S_2). The scale bar represents 0.5 μm.

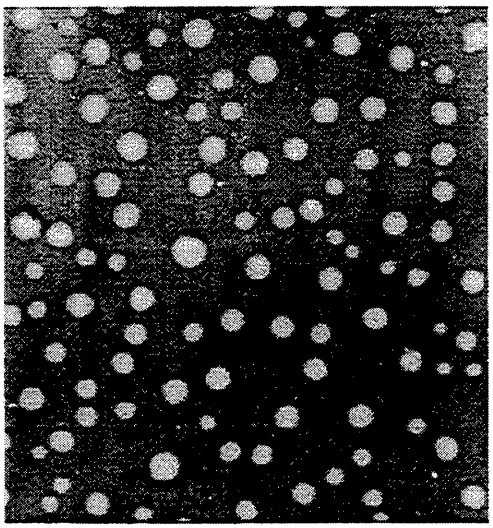

Figure 4-2 A TEM micrograph of aluminosilicate particles (before esterification). The scale bar represents 0.5 μm.

Table 4-2 Silica(S) and aluminosilicate (A) particle size and zeta potential.

Type	DLS Diameter (nm)	TEM Diameter (nm)	Zeta Potential (mV)	Conductance (μS)
S_b	430±48	350±20	-54.6	33.0
S_a	440±45	357±15	-37.3	28.6
A_b	398±107	242±91	-33.7	76.9
A_a	438±91	-	-24.9	36.5

S_b and S_a represent silica particles before and after esterification.

A_b and A_a represent aluminosilicate particles before and after esterification

4.3.3 Spectroscopy

To determine the local structure of aluminosilicate particles, infrared spectroscopy and nuclear magnetic resonance were used and are discussed in the following sections.

4.3.3.1 Infrared Spectroscopy

In order to confirm that the obtained aluminosilicate particles are indeed a mixture of SiO_2 and Al_2O_3, infrared spectroscopy (IR) was introduced to characterize functional groups within the particles.

The solid silica and aluminosilicate colloidal particles were analyzed by Fourier transform infrared spectroscopy (FTIR)[FTS-40, BioRad], using potassium bromide as the background. Both the silica IR spectrum and the aluminosilicate IR spectrum are plotted for comparison in Figure 4-3. The major differences in these spectra are located at wavenumbers lower than 1,200 cm^{-1}, details of which are shown in Figure 4-4. To interpret the functional groups present in each sample, the wavenumber of each peak in the lower region is compared to the values from Banerjee [104] and Hirata [105] as shown in Table 4-3.

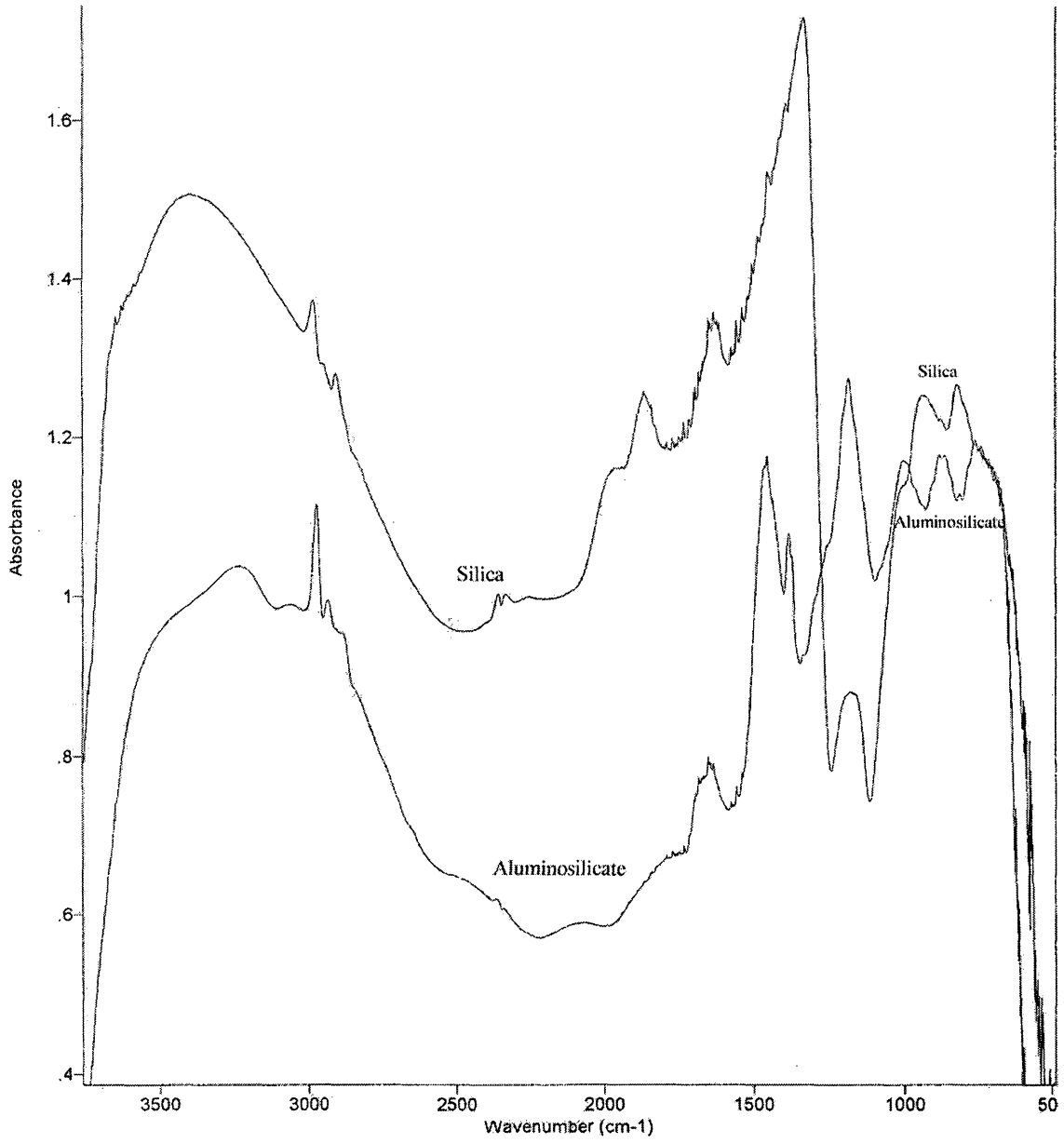

Figure 4-3 IR spectrum of silica and aluminosilicate.

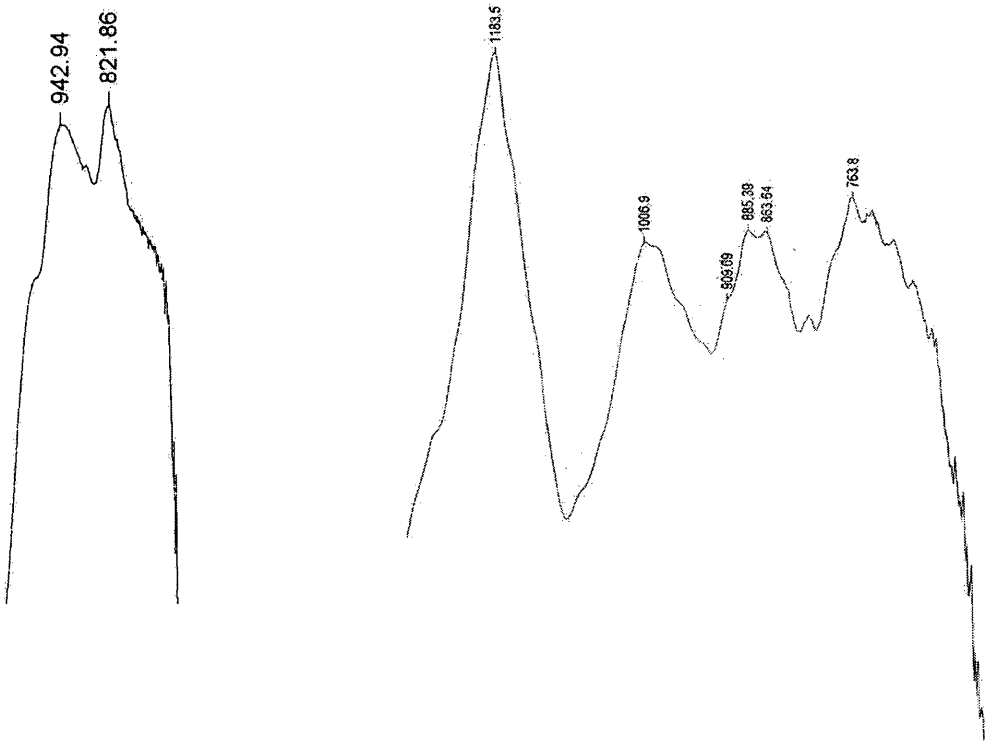

Figure 4-4 (i) IR spectrum of silica and (ii) IR spectrum of aluminosilicate.

Table 4-3 Interpretation of silica and aluminosilicate IR spectra.

Substance	**Functional group**	**Wavenumber (cm^{-1}) (observed)**	**Wavenumber* (cm^{-1})**
Silica	Si-OH	942.9	835-955
	$Si-OC_2H_5$	821.9	800-810
Aluminosilicate	Si-OH	885.4	835-955
	SiO_4	909.7	900-920
		-	1100-1150
		1183.5	1165-1180
	AlO_4	763.8	735-740
		863.6	810-825
	Al-O-Si	1006.9	1010

* [104], [105]

By comparing wavenumbers obtained from the IR aluminosilicate spectrum to the values from literature, we can safely say that

1. there are Al-O-Si and Si-OH bonds present in the aluminosilicate
2. Al is present in a tetrahedral structure, and
3. Si is also present in a tetrahedral structure.

4.3.3.2 Nuclear Magnetic Resonance

Though IR is clearly useful for structure characterization, it does not tell us the complete story. In order to further analyze the aluminosilicate structure, three types of nuclear magnetic resonance (NMR) studies were performed, including ^{29}Si, ^{27}Al, and ^{1}H NMR. A ^{29}Si NMR spectrum for aluminosilicate is shown in Figure 4-5. Here, a peak is found at -89.6 ppm corresponding to the ^{3}Q structure. This tells us that there are Si atoms connected to three other heavy element atoms via oxygen linkages and one OH linkage. To the left of this peak, there is a shoulder at -65.8 ppm corresponding to the ^{1}Q structure. Here, Si atoms are surrounded by three OH linkages and one heavy element atom connected to oxygen [106].

From the obtained ^{27}Al NMR spectrum shown in Figure 4-6, there are two peaks present at 4.7 and 57 ppm, corresponding to octahedral and tetrahedral (^{4}Q) coordinations, respectively [106]. In the octahedral structure, Al will be surrounded by H or any heavy element atoms connected to oxygen, while in the ^{4}Q structure, Al will be surrounded only by heavy element atoms with oxygen linkages. By integrating the area under both peaks, it was found that the ratio of tetrahedral to octahedral structure in Al is ~1.55. Moreover, when comparing the total peak area to the peak area of the standard aluminum nitrate, the percent weight of Al in the aluminosilcate particles can be approximately determined. From this, it is found that there is approximately 18±5 wt% Al present.

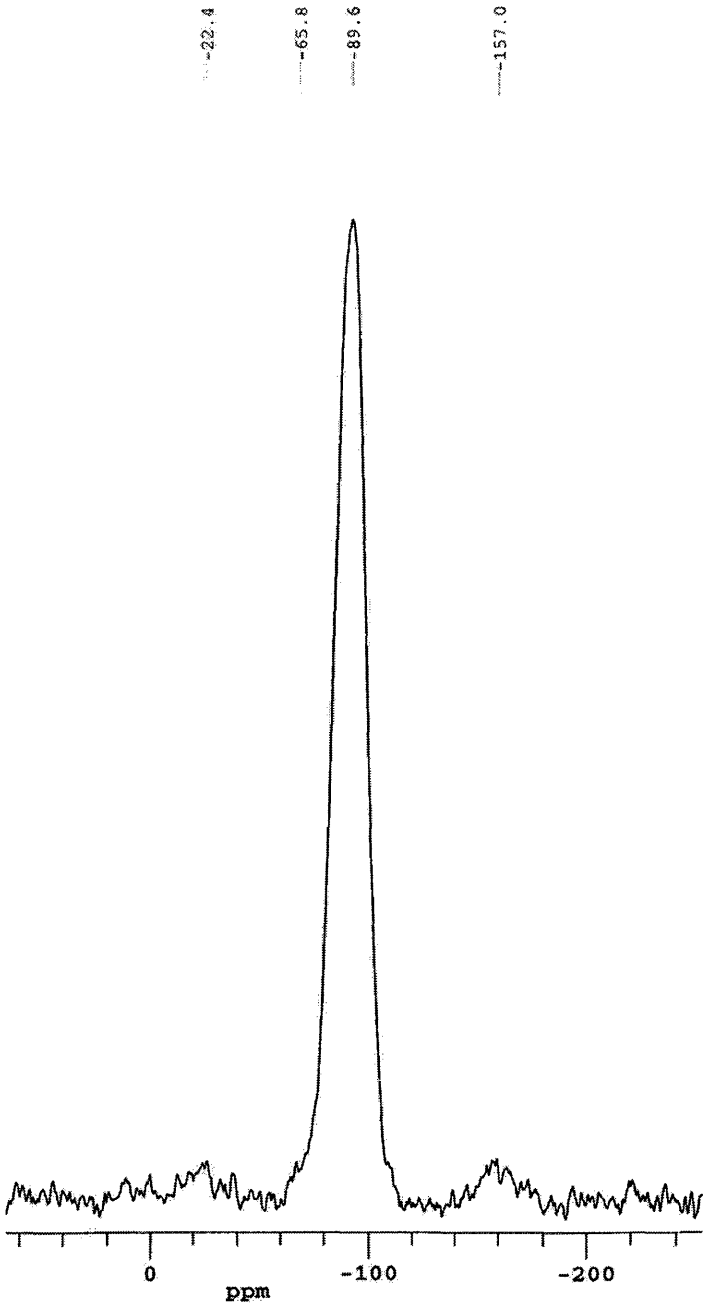

Figure 4-5 ^{29}Si NMR of aluminosilicate.

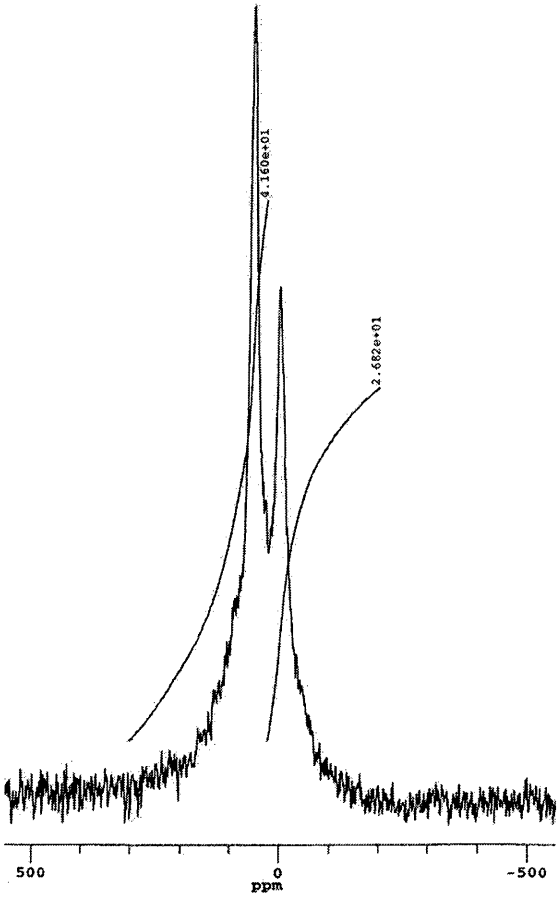

Figure 4-6 ^{27}Al NMR of aluminosilicate.

From the ^{1}H NMR spectrum shown in Figure 4-7, it is apparent that peaks are present at 0.9 ppm and in the range of 3.5-5.2 ppm. The peak at 0.9 ppm corresponds to the silanol proton and peaks in the range of 3.5-5.2 ppm indicate the presence of physisorbed water within the aluminosilicate particles [107].

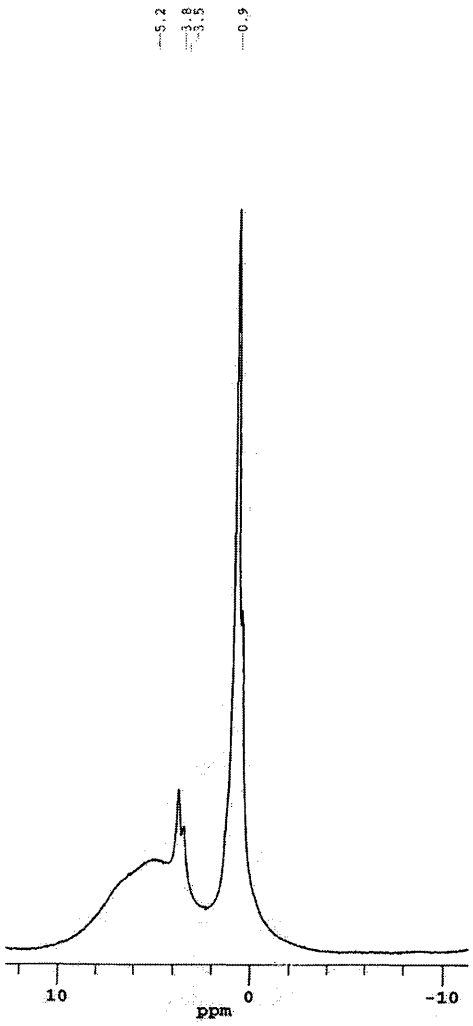

Figure 4-7 ^{1}H NMR of aluminosilicate.

4.3.4 Thermogravimetric Analysis

As discussed above, ^1H NMR studies indicate the presence of water in the aluminosilicate. In order to determine the quantity of water in the structure, thermogravimetric analysis (TGA) [TG/DTA 220, Seiko] was introduced. Shown in Figure 4-8 are the results determined from TGA measurement by heating the aluminosilicate sample of known weight at a rate of 10°C/min under He atmosphere. From this curve, it appears that there is approximately 31% weight loss. By looking at differential thermogravimetric (DTG) and differential thermal analyzer (DTA) curves, it is found that 10.4% weight loss has occurred between 25-144 °C, corresponding to the AB peak on the DTG curve and the first minimum on the DTA curve. Since this temperature range corresponds to the boiling point of water, 10.4% suggests that approximately two molecules of water are present in the structure $Al_2O_3.2SiO_2$ (this structure is based on the Al:Si mole ratio present in the aluminosilicate ester reactant). Also, a peak at 14.6% weight loss occurred in the temperature range of 144-273 °C corresponding to the BC peak on the DTG curve and the second minimum on the DTA curve. This temperature range corresponds to dehydroxylation (150-550 °C) according to the studies of Fitzgerald [108].

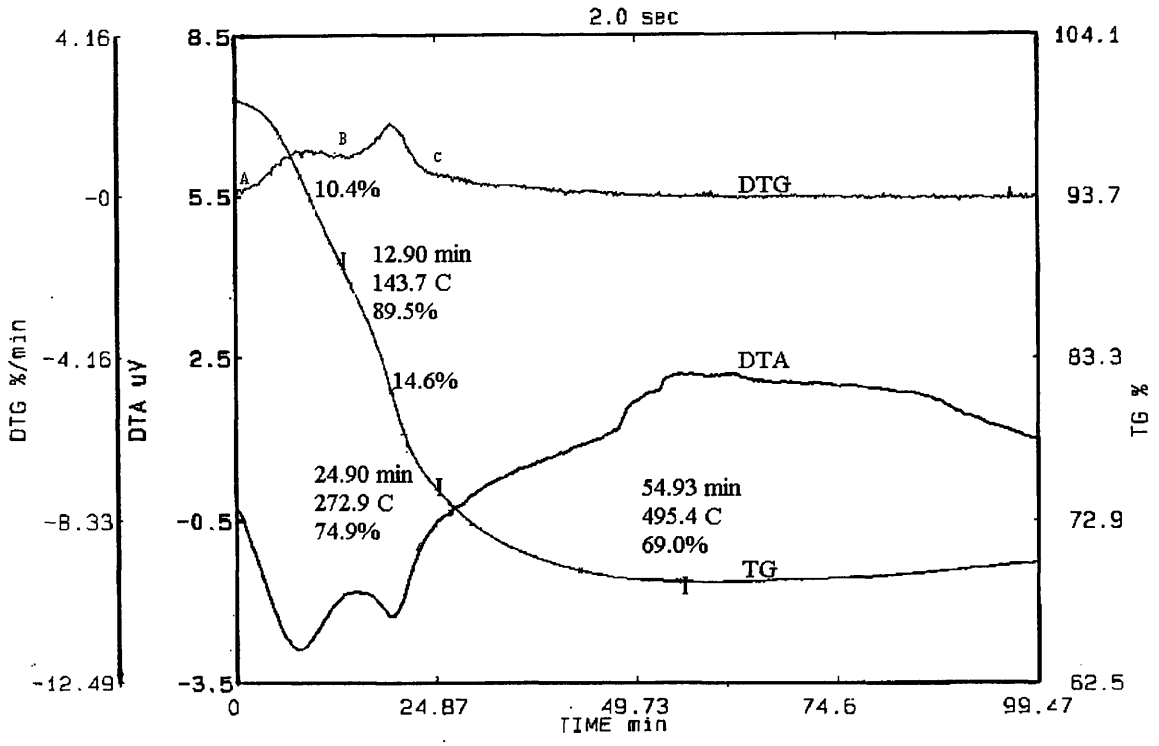

Figure 4-8 Thermogravimetric analysis.

4.3.5 Index of Refraction Measurement

To determine the refractive index of silica and aluminosilicate particles, a series of stock solutions having various indices of refraction was prepared. By mixing ethanol (n=1.3605) with toluene (n=1.4946), and mixing toluene with *o*-dichlorobenzene (n=1.5510), the refractive indices of the stock solutions were varied between 1.40 and 1.55.

A simple light scattering geometry was set up and the sample transmission measured for the silica and aluminosilicate suspensions in the stock solutions of known refractive index. The transmission was then plotted as a function of refractive index as shown in Figure 4-9 and 4-10. The solvent index of refraction that provides the maximum transmission was taken as the particle index of refraction. From Figure 4-9 and 4-10, by fitting the transmission curves of silica and aluminosilicate particles with a simple parabolic function, it was found that the refractive index of silica is approximately 1.445±0.0001 and the refractive index of aluminosilicate is approximately 1.489±0.0007.

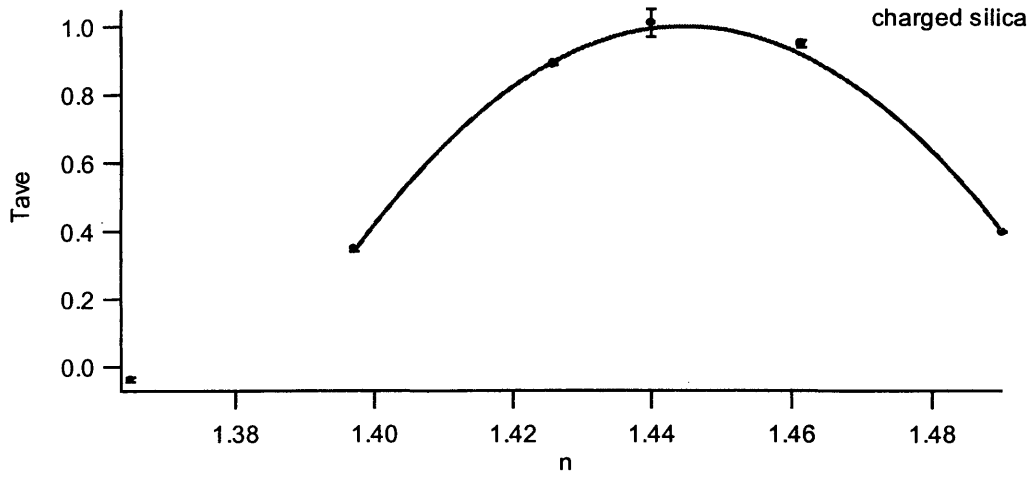

Figure 4-9 Silica index of refraction measurement.

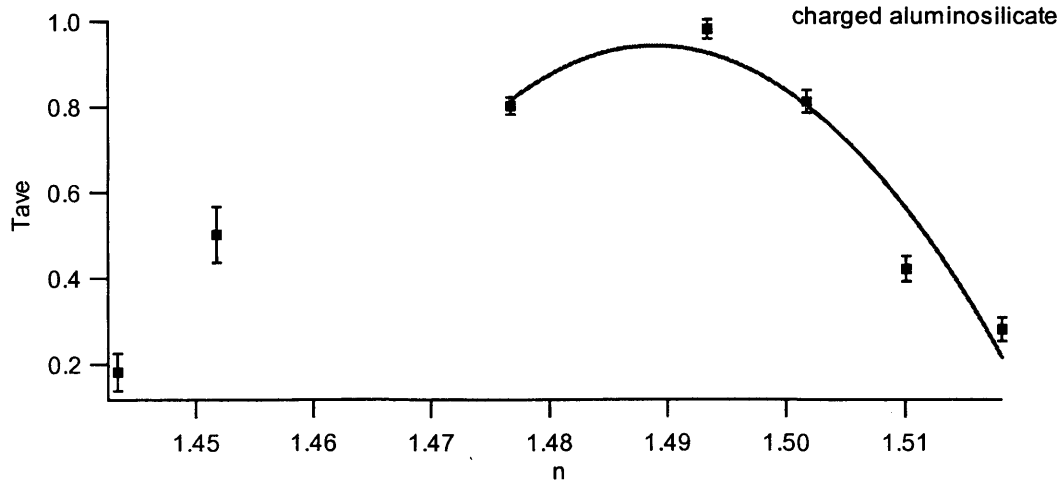

Figure 4-10 Aluminosilica index of refraction measurement.

4.4 Light Scattering

In order to investigate the contrast variation model, scattering techniques are introduced. Our investigations were performed on both ordered and disordered systems; therefore, we will discussed both disordered phase scattering and ordered phase scattering, commonly known as diffraction. In scattering theory, the basic equations describing x-ray, neutron, and light scattering are similar. Due to the experiments we intend to carry out, the details will be discussed in the context of static light scattering. Light scattering geometry is shown is Figure 4-11.

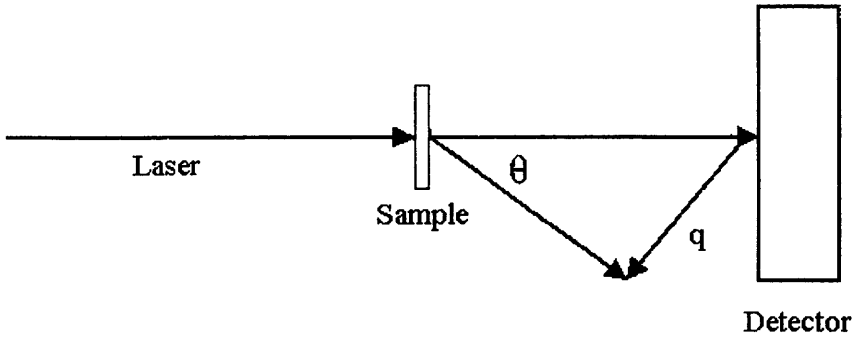

Figure 4-11 Static light scattering geometry

4.4.1 Theory

The basic theory of small angle x-ray scattering was given by Guinier and Fournet in 1955 [109], which is equivalent to the fundamental theory of light scattering. If we assume that both multiple and incoherent scattering are minimal, the scattering intensity per unit volume from a sample having p different kinds of scattering spheres is given by [66]

$$I(q) = \left\langle \left| \sum_{\alpha=1}^{p} \sum_{i=1}^{N_\alpha} b_\alpha(q) \exp\left(i\mathbf{q}r_i^\alpha\right) \right|^2 \right\rangle \qquad [4.1]$$

where,

N_α = the number of particles of type α

$b_\alpha(q)$ = the corresponding scattering amplitude

r_i^α = the position of particle i of type α

$$q = \frac{4\pi}{\lambda} \sin\frac{\theta}{2} = \text{the magnitude of the scattering wave vector } \mathbf{q} \qquad [4.2]$$

where θ = the scattering angle and λ = the wavelength of incoming light.

Typically, the scattering intensity is written in terms of the form factor $P(q)$ and the structure factor $S(q)$ via

$$I(q) \propto P(q)S(q) \qquad [4.3]$$

where

$S(q)$ is the structure factor due to interparticle correlations

$P(q)$ is the form factor, also called the intraparticle structure factor, which contains information about the size and shape of individual particles. For monodisperse spheres,

$$P(q) = \frac{9\pi}{2}\left[\frac{J_{3/2}(qa)}{(qa)^{3/2}}\right]^2 = \left[\frac{3\sin qa - qa\cos qa}{(qa)^3}\right]^2 \qquad [4.4]$$

where, a = the particle radius.

For systems composed of different scattering spheres, the scattered intensity can be written as [66]

$$I(q) = n\overline{P}(q)S^M(q) \qquad [4.5]$$

where

n = the total number density of the sample

$\overline{P}(q)$ = the averaged form factor

$S^M(q)$ = the measured structure factor containing information about the interparticle correlations of the sample.

For spherical particles of homogeneous scattering material, the averaged form factor is

$$\overline{P}(q) = \sum_{\alpha=1}^{p} x_\alpha b_\alpha^2(q) \qquad [4.6]$$

where, $x_\alpha = \frac{n_\alpha}{n}$ = the mole fraction of species α and

$$b_\alpha(q) = V_p^\alpha \left(n_p^\alpha - n_s\right) \frac{3J_1(qa_\alpha)}{qa_\alpha} \qquad [4.7]$$

where,

V_p^α = the volume of particle α

n_p^α and n_s = the refractive indices of particles α and of the solvent, respectively

a_α = the radius of particle α

J_1 = the first-order spherical Bessel function, which

$$J_1(qa_\alpha) = \sqrt{\frac{\pi}{2qa_\alpha}} J_{3/2}(qa_\alpha) \qquad [4.8]$$

$$\frac{3J_1(qa_\alpha)}{qa_\alpha} = \sqrt{\frac{9\pi}{2}} \frac{J_{3/2}(qa_\alpha)}{(qa_\alpha)^{3/2}} = \sqrt{P_\alpha(q)} \qquad [4.9]$$

The measured structure factor can be defined as

$$S^M(q) = \frac{1}{\overline{P}(q)} \sum_{\alpha=1}^{p} \sum_{\beta=1}^{p} b_\alpha(q) b_\beta(q) S_{\alpha\beta}(q) \qquad [4.10]$$

where,

$$S_{\alpha\beta}(q) = \frac{1}{N} \sum_{i=1}^{N_\alpha} \sum_{j=1}^{N_\beta} \left\langle \exp\left(i\mathbf{q}\left(r_i^\alpha - r_j^\beta\right)\right)\right\rangle = x_\alpha \delta_{\alpha\beta} + n x_\alpha x_\beta \tilde{h}_{\alpha\beta}(q) \qquad [4.11]$$

$S_{\alpha\beta}$ = the partial structure factors

$\delta_{\alpha\beta} \cong S_{\alpha\beta}$ for q larger than q^m where $S_{\alpha\beta}$ maximum occurs

$\tilde{h}_{\alpha\beta}(q)$ = the Fourier transform of the total correlation function $h_{\alpha\beta}(r)$

N = the total number of particles

For a dilute (non-interacting) system of density n_0, $\tilde{h}_{\alpha\beta}(q)$ goes to zero and the measured structure factor approaches unity; therefore, the corresponding measured intensity becomes

$$I_0(q) = n_0 \overline{P}(q) \qquad [4.12]$$

In a binary mixture, the measured structure factor can be obtained from the light scattering data via

$$S^M(q) = \frac{I(q) n_0}{I_0(q) n} \qquad [4.13]$$

$$= \frac{1}{\overline{P}(q)} \left[b_1^2(q) S_{11}(q) + b_2^2(q) S_{22}(q) + 2 b_1(q) b_2(q) S_{12}(q) \right] \qquad [4.14]$$

from which the partial structure factor can be extracted from

$$S_{12}(q) = \frac{S^M(q)\overline{P}(q) - b_1^2(q) S_{11}(q) - b_2^2(q) S_{22}(q)}{2 b_1(q) b_2(q)} \qquad [4.15]$$

4.4.1.1 Experiments

In our contrast variation experiments, we have prepared colloids in the diameter range of 200 to 500 nm. From Equation 4.2, if we are to use visible light to study colloidal distribution on these length scales, the scattering angle must be relatively large.

To perform such studies, a wide angle light scattering (WALS) apparatus was constructed as shown in Figure 4-12.

In this, a HeNe laser of wavelength 632.8 nm is directed through hole A at the sample holder, then reflected at a 90° angle, and then passed through the sample vial. Transmitted light is reflected again at 90° to leave the sample holder at hole B. Scattered light is projected on a screen and the images captured by a 2-dimensional camera [Detector Controller TEA/CCD-512 EFT, Princeton Instruments, Inc]. A moving belt with a slit was used to allow the camera to capture the scattering intensity at a particular angle more efficiently and without interference from other angles, avoiding an effect called "smearing". Due to the screen curvature, the scattering intensity could be measured only over a range of 60-120°, equivalent to a q range of 0.01-0.017 nm^{-1}.

In order to study binary mixtures, three different mixtures of known volume fraction of silica and aluminosilicate particles were suspended in solvents of different index of refraction. System one was of intermediate index solvent in which both particle types scattered light. System two is index-matched for silica and system three is index-matched for the aluminosilicate.

In our studies, we use three solvents, including ethanol, benzene and cyclohexane and examine two kinds of particles, including charged and esterified colloids. Zeta potential measurements of silica and aluminosilicate particles in water discussed in Section 4.3.2 show the decrease in surface potential after esterification. This illustrates the removal of some OH group at the particle surface and their replacement by octadecyl

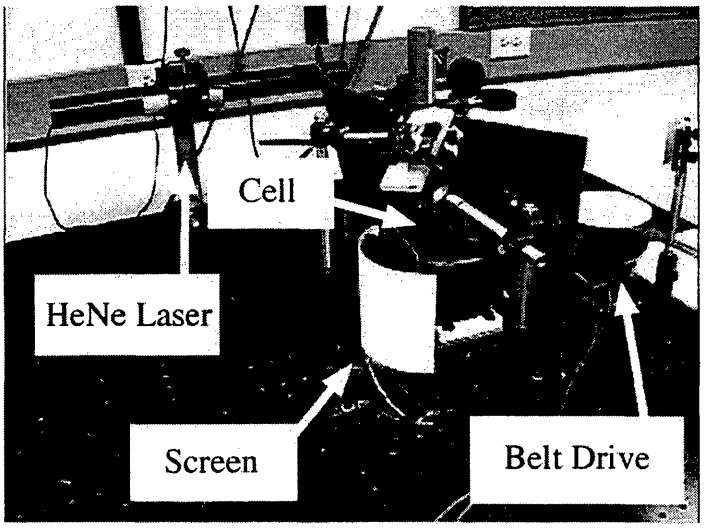

(a)

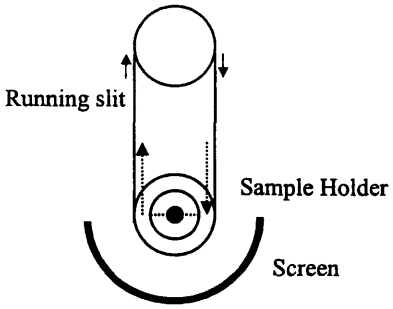

(b)

ARTHUR LAKES LIBRARY
COLORADO SCHOOL OF MINES
GOLDEN, CO 80401

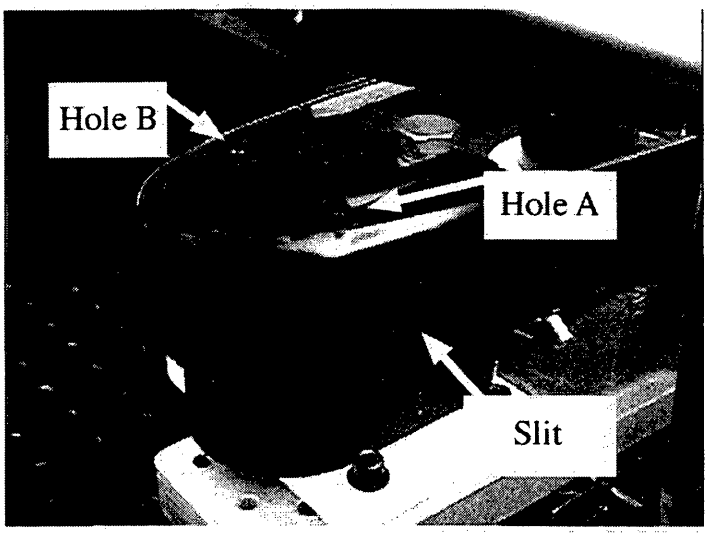

(c)

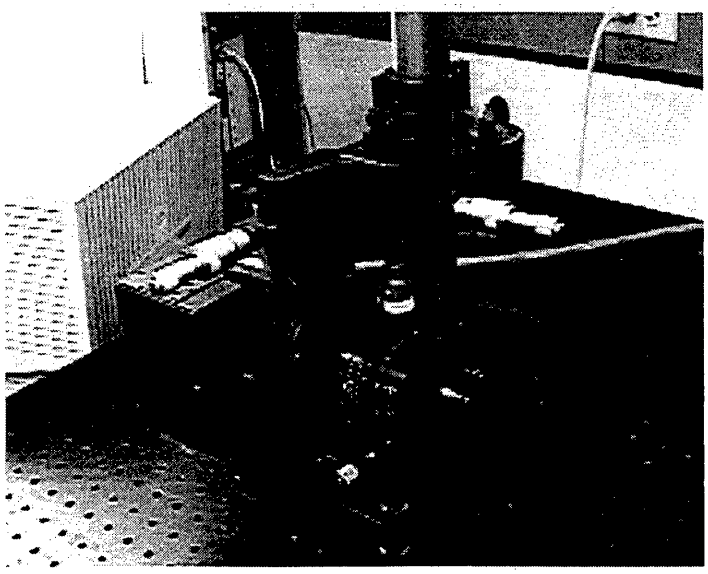

(d)

Figure 4-12 (a) WALS setup, (b) Top view of the WALS setup (c) Sample cell, and (d) Detector.

chains after the esterification reaction is performed. By removing surface charge through polymer grafting onto the surface, the charge-charge interaction between particles can be decreased. However, this interaction will be further decreased when the particles are dispersed in nonpolar solvents, making the particles nearly hard-sphere like. For fully charged particles, OH groups at the surface induce a charge-charge interaction, providing long-range repulsions. When dispersed in nonpolar solvents, the charge-charge interaction decreases less than in the esterified systems.

Table 4-4 Physical properties of silica, aluminosilicate, and solvents.

Particles	**Refractive index**	**Density (g/cm^3)**
silica	1.45	2.2
aluminosilicate	1.49	2.1±0.2
Solvents		
benzene	1.50	0.88
cyclohexane	1.43	0.78
ethanol	1.36	0.79
toluene	1.50	0.87

* from pcynometry

** from transmission measurements in Section 4.3.5

the other valves obtained from CRC Handbook, 62nd Editon

To prepare model binary mixtures, the physical properties of both particles and solvents used must be known and are listed in Table 4-4. A listing of the binary systems investigated is given in Table 4-5.

Table 4-5 Binary systems studied by contrast variation.

Particles	**Solvents**		
	System 1	**System 2** **volume ratio**	**System 3** **volume ratio**
esterified silica/aluminosilicate	ethanol	ethanol /toluene 1:1.67 (1.45)	ethanol/toluene 1:21.42 (1.49)
	benzene	ethanol/benzene 1:1.49 (1.44)	ethanol/benzene 1:10.71 (1.49)
	cyclohexane	cyclohexane/toluene 1:0.37 (1.45)	cyclohexane/toluene 1:11.25 (1.49)
charged silica/aluminosilicate	ethanol	ethanol /toluene 1:1.67 (1.45)	ethanol/toluene 1:21.42 (1.49)

Values in parenthesis represent the calculated refractive indices.

4.4.1.2 Results

After the 2-D scattering data is captured from the screen, the image is reduced and averaged to produce a 1-D plot of measured intensity as a function of scattering angle. After subtracting the background intensity arising from solvent contributions, the data is normalized to correct for curvature and the relative scattering intensity of a particular dispersion is plotted as a function of q.

In very dilute systems, the structure factor approaches unity and the scattering intensity is proportional only to the form factor. In order to measure the form factor and determine particle size, single component systems of dilute silica and aluminosilicate in ethanol were investigated. When the measured scattering curves were fitted to the form factor predicted for monodisperse spheres, particle sizes were obtained as shown in Table 4-6 and Figures 4-13 through 4-16.

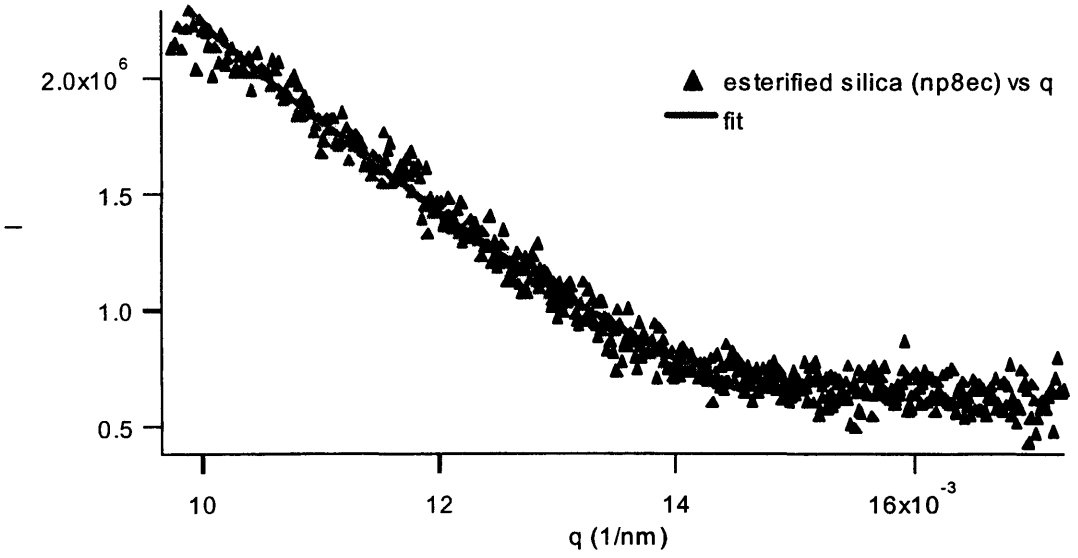

Figure 4-13 Scattering intensity of dilute esterified silica in ethanol.

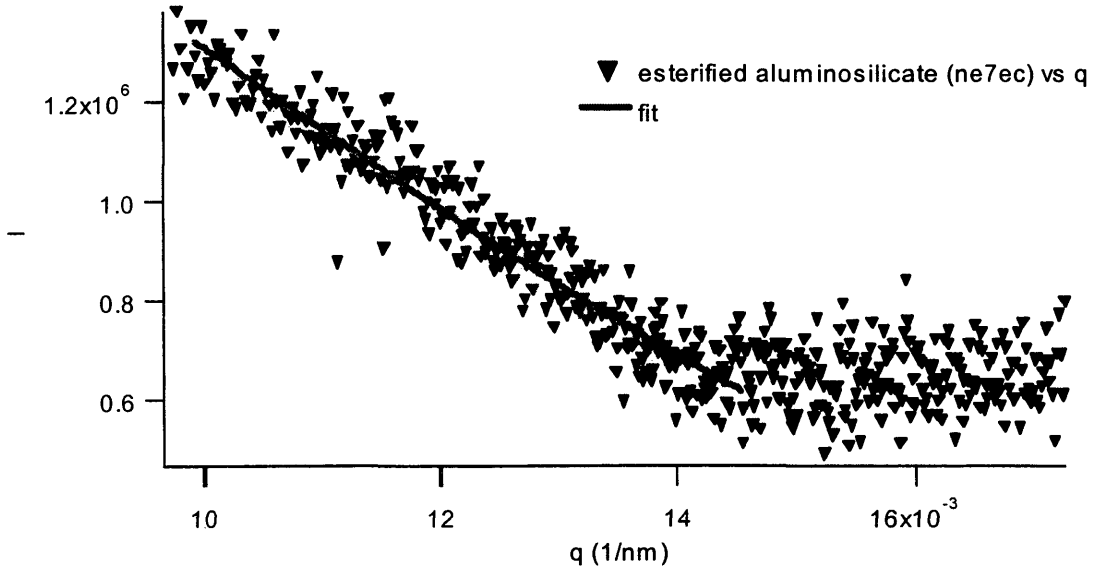

Figure 4-14 Scattering intensity of dilute esterified aluminosilicate in ethanol.

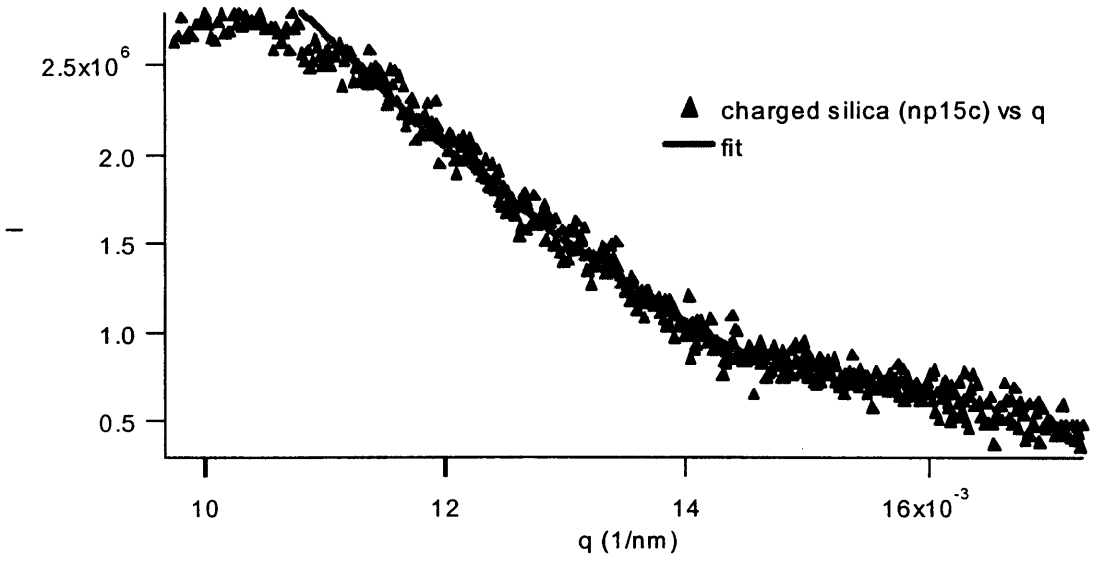

Figure 4-15 Scattering intensity of dilute charged silica in ethanol.

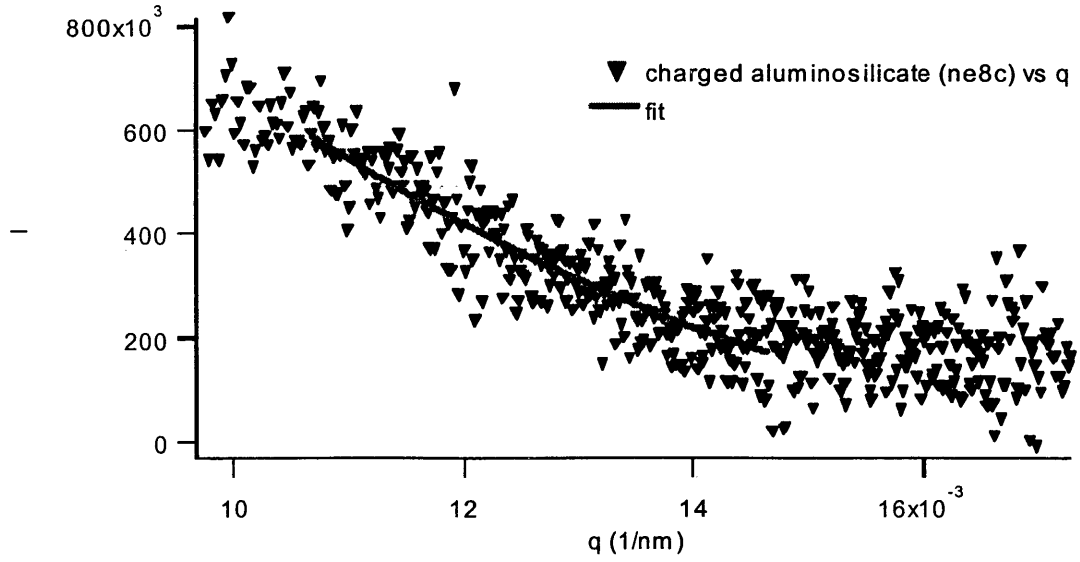

Figure 4-16 Scattering intensity of dilute charged aluminosilicate in ethanol.

Table 4-6 WALS particle sizes of dilute single component systems in ethanol.

Particles (Batch #)	**Radius (nm)**
esterified silica (np8ec)	207±5
esterified aluminosilicate (ne7ec)	170±10
charged silica (np15c)	216±5
charged aluminosilicate (ne8c)	214±17

For binary systems, the scattered intensity from dilute mixtures in solvents of intermediate index will provide the averaged form factor and the mixed particle size using Equation 4.12. In analogy with Equation 4.13, and denoting silica as 1 and aluminosilicate as 2, $S_{11}(q)$ and $S_{22}(q)$ can be extracted by dividing the system 3 scattering intensity (index-matched for aluminosilicate) and system 2 scattering intensity (index-matched for silica) with the scattering intensity of single component silica and aluminosilicate, respectively. From Equation 4.15, by using the obtained $S_{11}(q)$ and $S_{22}(q)$ with the averaged form factor, $S_{12}(q)$ can be determined.

Table 4-7 Particle sizes of dilute binary mixtures from WALS.

Particles (Batch#)	**Solvent**	**Radius (nm)**
esterified silica (np8ec)+ esterified aluminosilicate (ne7ec)	benzene	288±6
	cyclohexane	233±16
	ethanol	219±5
charged silica (np15c) + charged aluminosilicate (ne8c)	ethanol	206±10

From Table 4-7, the particle sizes of dilute mixtures of esterified silica and esterified aluminosilicate in benzene is higher than particle sizes from individual measurements. This indicates a tendency for particle aggregation as seen in previous studies [54, 110] where it is mentioned that attractions are introduced in dispersions of hard spheres in benzene. For cyclohexane and ethanol solvents, particle sizes appear smaller indicating a lack of aggregation behavior.

A FORTRAN program has been made available for calculating the direct correlation function for hard sphere mixtures [111]. As discussed previously, direct correlation functions are directly related to the partial structure factors; therefore, results can be used to compared to our WALS measurements. Plots showing the calculated and

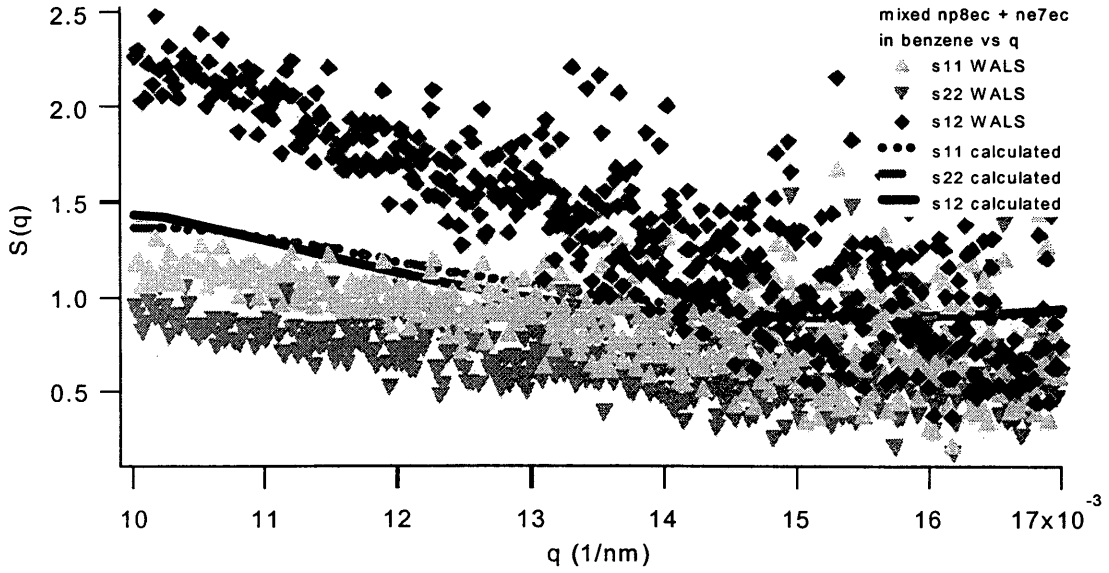

Figure 4-17 Binary mixture of esterified silica and esterified aluminosilicate in benzene.

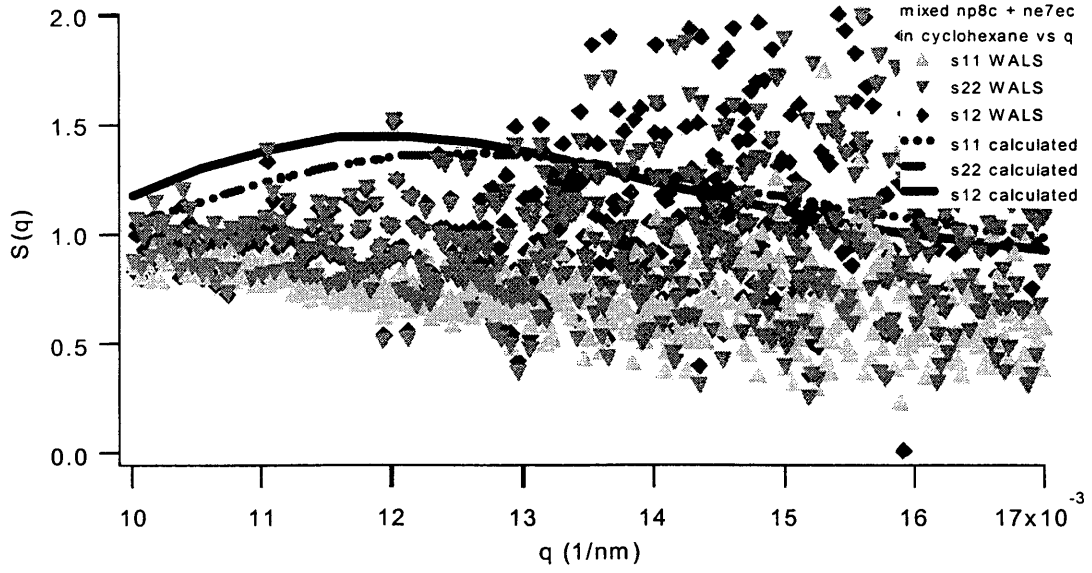

Figure 4-18 Binary mixture of esterified silica and esterified aluminosilicate in cyclohexane.

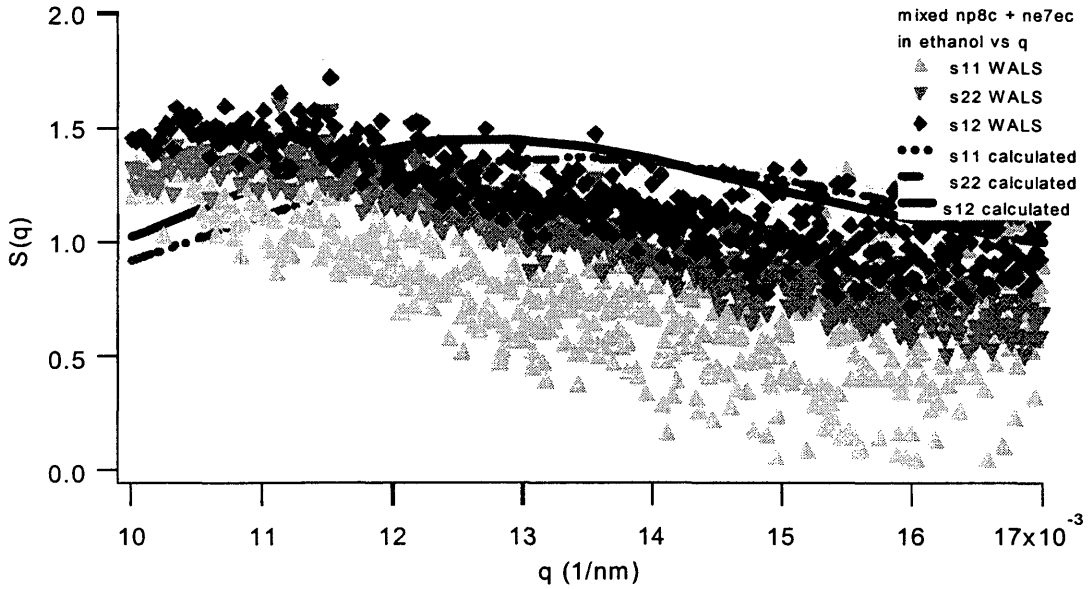

Figure 4-19 Binary mixture of esterified silica and esterified aluminosilicate in ethanol.

measured partial structure factors, $S_{11}(q)$, $S_{22}(q)$, and $S_{12}(q)$, for the binary mixtures as listed in Table 4-5 are shown in Figures 4-17 through 4-19.

Figure 4-17 shows the measured structure factors of a binary mixture of esterified silica and esterified aluminosilicate in benzene, where a steep slope in S_{12} is evident. This shows the difference in structure between system 2 (for S_{22}) and system 3 (for S_{11}). In system 1, the mixture is suspended in pure benzene where there is a possibility for aggregation to occur. Whereas, in systems 2 and 3, ethanol is added to the mixture for index-matching, changing the solvent and slightly modifying the particle-particle interactions.

Our experimental results are lower in magnitude for S_{11} and S_{22} than results from thermodynamic calculation. This could be a result of our volume fraction values; in our experiments, the dispersion is initially dispersed but then sediments increasing the local volume fraction. As the laser passes through this location, the local volume fractions must be estimated. Predicted structure factors are computed using these estimated volume fractions leading to some error in the magnitude of S_{11} and S_{22}.

From Figure 4-18, for mixtures of esterified silica and esterified aluminosilicate in cyclohexane, there is good agreement between the experimental structure factors and the results from calculation except for the magnitude. This difference could arise from the volume fraction approximation as mentioned earlier, or from fluctuations in experimental data at high q where the scattering intensity is low leading to large errors after subtracting the background.

In mixtures of esterified silica and esterified aluminosilicate in ethanol as shown in Figure 4-19, experimental results had similar magnitudes to predictions, however, there is a difference in the peak location. Here, we normalize the calculated curves by the radius obtained from the dilute mixed systems, which may not be accurate. If we adjust the radius, we can bring the results from both approaches into good agreement.

For binary mixtures of charged silica and charged aluminosilicate in ethanol, there were experimental difficulties due to large fluctuations. There most likely arose because of the low local density of the sample. OH groups at the silica surface will prevent close colloidal contact due to charge-charge interactions. As light passes through the sample, this results in less scattering. This hypothesis is based on the relatively large average lattice parameters determined for ordered single component silica colloids obtained from diffraction.

4.4.2 Light Diffraction

For ordered systems, incoming light will diffract at a specific angle depending on crystal orientation. Using light of known wavelength λ, and by measuring the angle θ as shown in Figure 4-20, one can determine the spacing d between planes of a crystal using Bragg's law, which can be expressed as [112]:

$$n\lambda = 2d\sin\theta \qquad [4.16]$$

where,

n = the order of reflection

λ = the wavelength of light

θ = the diffracting angle

d = spacing between planes of a crystal

For a cubic lattice, the d spacing can be related to the lattice parameter, a, by

$$\frac{1}{d^2} = \frac{h^2 + k^2 + l^2}{a^2}. \qquad [4.17]$$

Defining

$$Q^2 = \frac{1}{d^2} \qquad [4.18]$$

leads to,

$$a = \left[\frac{h^2 + k^2 + l^2}{Q^2}\right]^2.$$

For each measured θ, using Equation 4.16, d and Q can be calculated. By normalizing all the Q values with the smallest Q, the summation of h, k, and l can be calculated. This leads to the determination of a as shown in Section 4.4.2.2 and the lattice structure by comparing to the known $h^2+k^2+l^2$ values of each structure. For example, peaks will be present when the h, k, and l values are all odd or all even for FCC lattice.

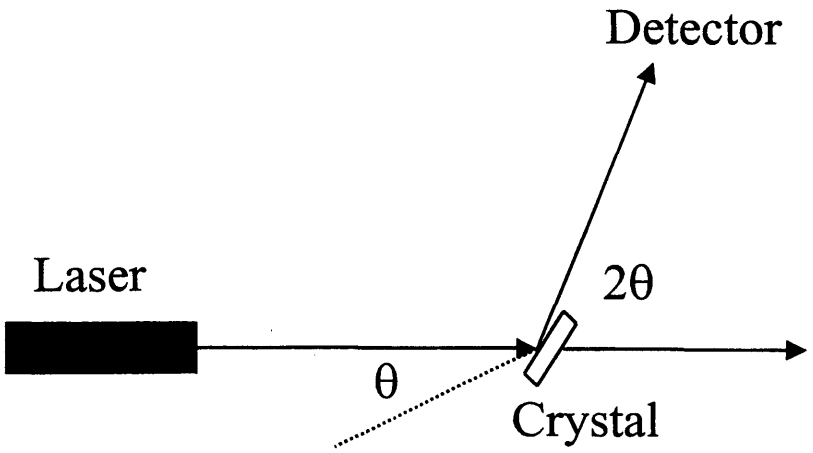

Figure 4-20 Light diffraction geometry.

4.4.2.1 Experiments

Light diffraction measurements were performed in a similar fashion to the WALS measurements. By placing a convex lens in front of the sample holder however, the laser beam was focused to a smaller diameter at the focal point.

In order to study ordered binary mixtures, silica and aluminosilicate dispersions were prepared in ethanol and mixed with toluene using the ratios presented in Table 4-5. After systems 1, 2, and 3 were prepared, they were transferred into a 3mm diameter NMR tube and sealed. These dispersions were subsequently left undisturbed for sedimentation and crystallization.

For single component studies, silica and aluminosilicate particles were dispersed in ethanol. Since there is a large contrast between silica and ethanol and aluminosilicate and ethanol, toluene was added to the dispersion to lower the contrast and to make the diffraction measurements feasible. Each suspension was then transferred to a 3mm diameter NMR tube, sealed, and left undisturbed for sedimentation and crystallization.

4.4.2.2 Results

For our single component studies, crystallization was present in both the charged silica system and in the esterified silica system. There was no crystallization observed in the aluminosilica systems. Crystals of charged silica were then investigated by light diffraction and the lattice parameter, a, determined. Results are listed in Table 4-8, where the diffraction intensities are compared to theoretical predictions for the FCC structure as shown in Figure 4-21.

Table 4-8 Lattice parameter calculation.

2θ	θ	d	$Q^2=1/d^2$	Q_n/Q_1	Ratio	h	k	l	a (nm)
54.5	27.25	691.0	2.0942E-06	1	3.00	1	1	1	1196
60	30	632.8	2.4973E-06	1.192	3.57	2	0	0	1265
102	51	407.1	6.033E-06	2.880	8.64	2	2	1	1221
115	57.5	375.1	7.1053E-06	3.392	10.18	3	1	0	1186
128.5	64.25	351.2	8.1037E-06	3.869	11.61	2	2	2	1216

a_{ave}1217

These results indicate an FCC lattice with a lattice parameter of 1217 nm. For esterified silica crystals, observed peaks at 45° and 148° were not enough to determine the crystal structure. We believe that no crystals were observed in the aluminosilicate system because of the high polydispersity in particle size.

For our binary studies, crystallization was only observed in mixtures of charged silica and charged aluminosilicate with the solvent index-matched for silica. Peaks were observed at 67°, 71°, and 133°, giving insufficient data once again to determine the crystal structure.

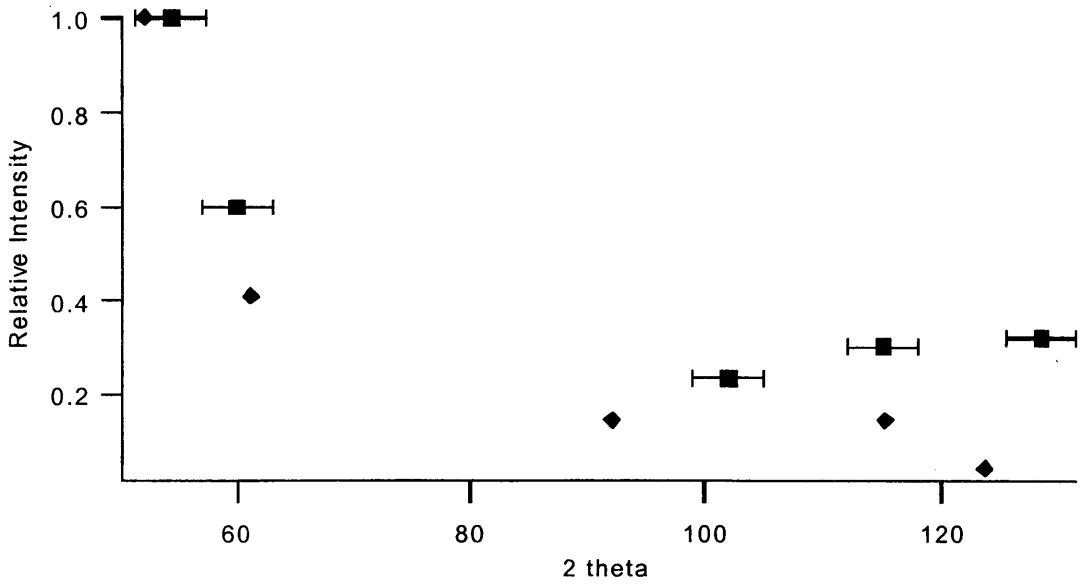

Figure 4-21 ◆Predicted diffraction intensity of charged silica ■ Experimental values.

CHAPTER 5

CONCLUSIONS AND PROPOSAL FOR FUTURE WORK

In these studies we have chosen colloids for the development of experimental models for the investigation of binary systems. With their variable surface properties and dispersing behavior in solvents, colloidal particles can represent theoretical models with both short and long-ranged interactions. Two models have been developed to investigate the structure of binary systems using two different experimental techniques.

One technique we have used is optical trapping, which requires a mismatch in refractive index between particles and solvents. In order to have a short-ranged interaction however, the difference in index of refraction between particles and solvent must be minimized. Two different kinds of colloids were therefore prepared, including silica and silica-coated titania, known as a "core-shell" model. With the index of refraction mismatch between the solvents and the titania core, core-shell particles are trappable, and by index-matching the silica shell with the solvent, the interactions remained short-ranged. Preliminary investigations via optical trapping were performed in mixtures of silica and silica-coated titania particles suspended in silica index-matching solvents. It was found that core-shell particles could be clearly seen and were trappable; whereas, the silica particles were only slightly visible and could not optically manipulated.

In these studies, however, some difficulties were encountered. For example, due to the high density of the core-shell colloids, particles quickly settled and adhered to the glass surface. Since the particle density is so high, there is no equivalent-density solvent available. For future work, in order to overcome difficulties during trapping, smaller silica-coated titania particles and more viscous solvents should be used to decrease settling velocities.

The other technique we have employed is light scattering, once again requiring an index-mismatch between particles and solvents. To experimentally investigate binary mixtures using this technique, one must have two colloidal types each with a slight difference in refractive index. For these studies we have used experimental models composed of silica and aluminosilicate. Since their refractive indices are slightly different, by index matching for silica, information on the aluminosilicate distribution could be determined. In the same way, by index matching for aluminosilicate, the silica distribution could be studied.

Since we wish to prepare colloidal models with both short and long-ranged interactions, colloidal surface charges were manipulated by esterification or dispersing in specific solvents. Short-ranged interactions were introduced by grafting polymer chains onto the particle surface, or, by retaining the original OH groups on the surface, interactions between these particles can be long-ranged. To investigate binary mixtures, both kinds of colloids were dispersed in different solvents. Mixtures of esterified silica and esterified alminosilicate were dispersed in benzene, cyclohexane, and ethanol. The

behavior of esterified silica and esterified aluminosilcate mixtures in benzene was shown to be different than the same mixture dispersed in cyclohexane and ethanol. This was likely due to an aggregation that occurred in benzene, while there was no evidence for aggregation in cyclohexane and ethanol.

To validate some of our experimental observations of short-ranged interaction systems of silica-silica, aluminosilicate-aluminosilicate, and silica-aluminosilicate, we have compared our results to calculated values for binary hard sphere mixtures. It was found that mixtures in ethanol provided the best agreement, while mixtures in benzene and cyclohexane showed relatively large deviations from calculated values. For grafted-polymer stabilized colloidal particles, chain-solvent interactions are an interesting issue for further studies. These interactions can be altered by changing dispersing solvents or by changing temperature. In our studies, we have observed for these colloid types different behavior when they were dispersed in different solvents. Previous investigations have shown evidence of esterified silica in benzene showing an effective attraction on lowering temperature [54, 113], changing particle behavior from hard sphere to adhesive hard sphere like. Such studies could be expanded for binary mixtures. By slowly changing the temperature of stabilized colloidal mixtures dispersed in a specific solvent, variation in the phase behavior as attractive interactions are slowly introduced could be studied.

In addition to disordered systems, we have extended the use of light scattering to study ordered binary mixtures. In these investigations, diffraction has been observed;

however, we were not able to characterize the crystal structure in some cases. According to the crystallization studies of Yoshida [114] and Barlett [14], a polydispersity of approximately 5% or less is required for colloidal crystallization to proceed on reasonable time scales. To improve our crystallizations studies, size separation techniques should be introduced. One possible technique is centrifugal SPLITT fractionation, which has been developed for the separation of macromolecules and particles, including materials in the colloidal size range [115]. A schematic diagram of centrifugal SPLITT is shown in Figure 5-1, where substream a' with suspended particles enters the SPLITT cell at inlet a'. After substream a' is merged to substream b', there is an imaginary interface between the two substreams. When the b' flowrate is greater than that of a', the feed stream will be compressed into thin lamina between the inner wall and the imaginary interface. The axis of separation is along the thin channel, where the fast particles exit at the outer outlet b and the slow particles exit at outlet a. After materials are processed through a SPLITT cell with a single outlet splitter, two fractions are obtained. These include one with a transport coefficient greater than the designated cutoff value and the other with the transport coefficient lower than the designated cutoff value. Since the sedimentation coefficient is a function of the particle diameter, the designated cutoff value can provide a desirable particle size by adjusting the constituent flowrates and the field strength.

Another possible technique for size separation is gel electrophoresis. There has been evidence of using gel electrophoresis to separate colloids into fractions with high monodispersity [116]. Electrophoresis is generally a process where particles of effective

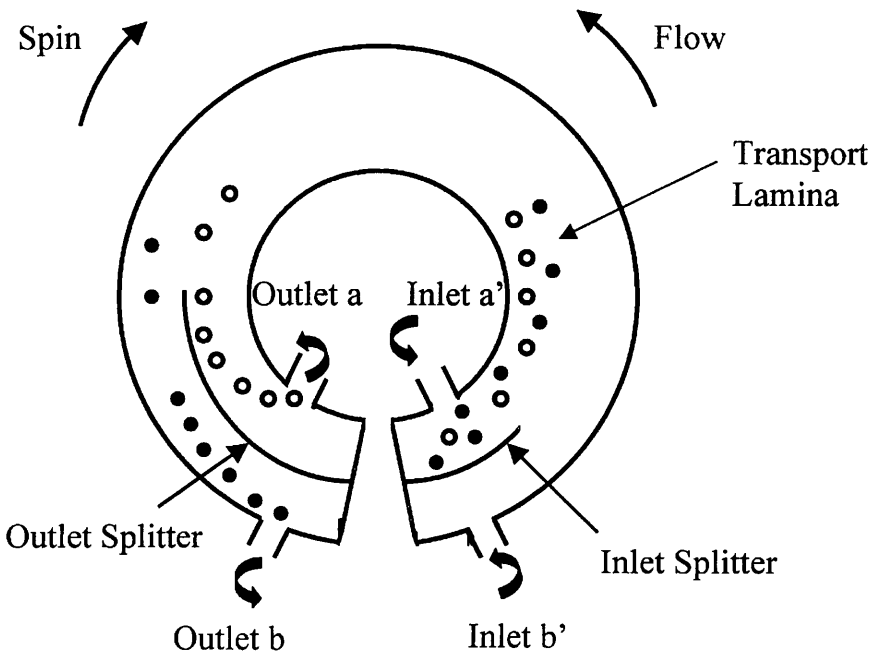

Figure 5-1 Centrifugal SPLITT.

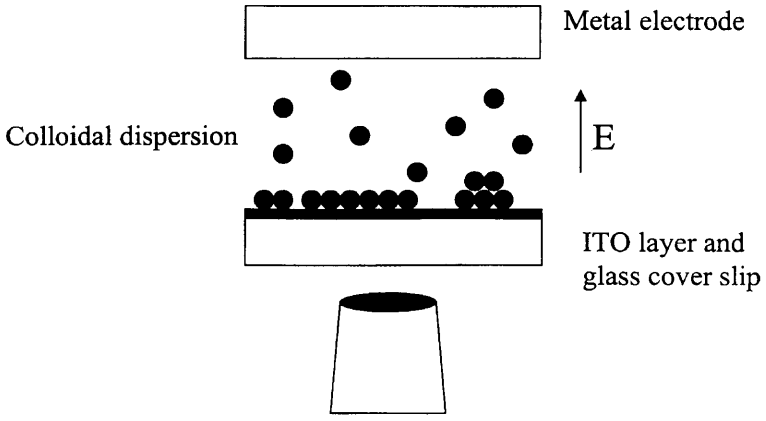

Figure 5-2 Electric field-induced colloidal crystallization

charge migrate in a medium under the influence of an electric field. In solution, particles are separated by their effective charge. Since gels have high viscosity and high frictional resistance, in gel electrophoresis, the particles are separated according to their size and charge providing standard deviations of 10% or less in particle size distribution.

In addition to speeding the crystallization process by increasing particle uniformity, electric fields can be used to directly induce colloidal crystallization. By introducing an electrohydrodynamic effect, it has been shown that the precise assembly of two and three-dimensional colloidal crystals on electrode surfaces can be created [117]. To observe the deposition, an optically transparent indium tin oxide (ITO) electrode is coupled to an optical microscope as shown in Figure 5-2. In the presence of an electric field, there will be a large electrostatic attraction between negatively charged particles and a positively charged electrode. When the applied voltage is increased sufficiently, particles will move toward the electrode surface. This attraction increases the particle density at the electrode creating colloidal crystals. Coalescence of these charged particles at the electrode surface is due to electrohydrodynamic fluid flow. Using this approach, it has been found that the assembly of three layers of polystyrene particles takes approximately 40 min with a 2 V applied voltage. Though crystal formation is reversible (when the electric field is removed, particles diffuse away by Brownian motion), this method could be used to overcome the kinetic barriers associated with colloidal crystal formation.

CHAPTER 6

REFERENCES

1. Dunning, W.J., *General and Theoretical Introduction.* Nucleation, ed. A.C. Zettlemoyer. 1969, New York: Marcel Dekker, Inc.
2. Cairns, R.J.R., Ottewill, R.H., *Studies on the Preparation and Properties of Lattices in Nonpolar Media.* J. Colloid Interface Sci., 1976. **54**(1): p. 45-51.
3. Salgi, P., *Polydispersity in Colloids: Implications to Static Structure and Scattering.* Advanced Colloid and Interface Science, 1993. **43**: p. 169-288.
4. van Megen, W., Pusey, P., Barlett, P., *Phase Behavior of Dispersions of Hard Spherical Particles.* Phase Transitions, 1990. **21**: p. 207-227.
5. Alder, B.J., Hoover, W.G., Young, D.A., *Studies in Molecular Dynamics V. High-Density Equation of State and Entropy for Hard Disks and Spheres.* J. Chem. Phys., 1968. **49**(8): p. 3688-3696.
6. Malijevsky, A., Veverka, J., *New Equations of State for Pure and Binary Hard-Sphere Fluids.* Phys. Chem. Chem. Phys., 1999. **1**: p. 4267-4270.
7. Kofke, D.A., *Solid-Fluid Coexistence in Binary Hard Sphere Mixtures by Semigrand Monte Carlo Simulation.* Molecular Simulation, 1991. **7**: p. 285-302.
8. Biben, T., Bladon, P., Frenkel, D., *Depletion Effects in Binary Hard-Sphere Fluids.* J. Phys.: Condens. Matter, 1996. **8**: p. 10799 - 10821.

9. Kranendonk, W.G.T., Frenkel, D., *Thermodynamic Properties of Binary Hard Sphere Mixtures.* Molec. Phys., 1991. **72**(3): p. 715-733.

10. Davidchack, R., Laird, B.B., *Simulation of the Binary Hard-Sphere Crystal/Melt Interface.* Phys. Rev. E, 1996. **54**(6): p. R5905-R5909.

11. Lebowitz, J.L., *Exact Solution of Generalized Percus-Yevick Equation for a Mixture of Hard Spheres.* Phys. Rev., 1964. **133**(4A): p. A895-A899.

12. Baxter, R.J., *Ornstein-Zernike Relation and Percus-Yevick Approximation for Fluid Mixtures.* J. Chem. Phys., 1970. **52**(9): p. 4559-4562.

13. Denton, A.R., Ashcroft, N. W., *Weighted-Density-Functional Theory of Nonuniform Fluid Mixtures: Application to Freezing of Binary Hard-Sphere Mixtures.* Phys. Rev. A, 1990. **42**(12): p. 7312-7328.

14. Barlett, P., Ottewill, R. H., Pusey, P. N., *Freezing of Binary Mixtures of Colloidal Hard Spheres.* J. Chem. Phys., 1990. **93**(2): p. 1299-1312.

15. Eldridge, M.D., Madden, P. A., *Binary Hard-Sphere Mixtures: A Comparison between Computer Simulation and Experiment.* Molec. Phys., 1995. **84**(2): p. 395-420.

16. Imhof, A., Dhont, J. K. G., *Experimental Phase Diagram of a Binary Colloidal Hard-Sphere Mixture with a Large Size Ratio.* Phys. Rev. Lett., 1995. **75**(8): p. 1662-1665.

17. Hiemenz, P.C., Rajagopalan, R., *Principles of Colloid and Surface Chemistry.* 1997, New York: Dekker.

18. Russel, W.B., *Colloidal Dispersions*. 1989, Cambridge U.K.: Cambridge Univ. Press.

19. Hogg, R., Healy, T.W., Fuerstenau, D.W., *Mutual Coagulation of Colloidal Dispersions*. Trans. Faraday Soc., 1966. **62**: p. 1638.

20. Ottewill, R.H., Hanley, H.J.M., Rennie, A.R., Straty, G.C., *Small-Angle Neutron Scattering Studies on Binary Mixtures of Charged Particles*. Langmuir, 1995. **11**: p. 3757-3765.

21. Genz, U., D'Aquanno, B., Mewis, J., Klein, R., *Structure of Sterically Stabilized Colloids*. Langmuir, 1994. **10**: p. 2206.

22. Goodwin, J.W., *Colloidal Dispersion*. 1982: Royal Society of Chemistry.

23. Fitch, R.M., *Polymer Colloids: a Comprehensive Introduction*. 1996: Academic Press.

24. Kranendonk, W.G.T., Frenkel, D., *Free Energy Calculations for Solid Solutions by Computer Simulations*. Molec. Phys, 1991. **72**(3): p. 699-713.

25. Kranendonk, W.G.T., Frenkel, D., *Computer Simulation of Solid-Liquid Coexistence in Binary Hard-Sphere Mixtures*. J. Phys.: Condens. Matter, 1989. **1**: p. 7735 - 7739.

26. Rovere, M., Pastore, G., *Fluid-Fluid Phase Separation in Binary Mixtures of Asymmetric Non-Additive Hard Spheres*. J. Phys.: Condens. Matter, 1994. **6**: p. A163-A166.

27. Lomba, E., Alvarez, M., *Phase Stability of Binary Non-Additive Hard-Sphere Mixtures: A Self Consistent Integral Equation Study.* J. Chem. Phys., 1996. **104**(11): p. 4180 - 4188.

28. Melnyk, T.W., Sawford, B. L., *Equation of State of a Mixture of Hard Sphere with Non-Additive Diameters.* Molec. Phys., 1975. **29**(3): p. 891-902.

29. Trizac, E., Eldridge. M. D., Madden, P. A., *Stability of the AB Crystal for Asymmetric Binary Hard Sphere Mixtures.* Molec. Phys, 1997. **90**(4): p. 675-678.

30. Napper, D.H., *Polymeric Stabilization of Colloidal Dispersions*, ed. R.H. Ottewill, Rowell, R. L. 1983, Sydney: Academic Press.

31. Cottin, X., Monson, P. A., *A Cell Theory for Solid Solutions: Application to Hard Sphere Mixtures.* J. Chem. Phys., 1993. **99**(11): p. 8914-8921.

32. Cottin, X., Monson, P. A., *Substitionally Ordered Solid Solutions of Hard Spheres.* J. Chem. Phys., 1995. **102**(8): p. 3354-3360.

33. Zeng, X.C., Oxtoby, D. W., *Density Functional Theory for Freezing of a Binary Hard Sphere Liquid.* J. Chem. Phys., 1990. **93**(6): p. 4357-4363.

34. Kerley, G.I., *Equations of State and Gas-Gas Separation in Soft Sphere Mixtures.* J. Chem. Phys, 1989. **91**(2): p. 1204-1210.

35. McQuarrie, D.A., *Statistical Mechanics*. 1976: Harper & Row.

36. Rick, S.W., Haymet, A. D. J., *Density Functional Theory for the Freezing of Lennard-Jones Binary Mixtures.* J. Chem. Phys., 1989. **90**(2): p. 1188-1199.

37. Mendez-Alcaraz, J.M., Aguanno, B. D., Klein, R., *Structure of Binary Colloidal Mixtures of Charged and Uncharged Spherical particles.* Langmuir, 1992. **8**: p. 2913-2920.

38. Rosenfeld, Y., *Free-Energy Model for the Inhomogeneous Hard-Sphere Fluid Mixture and Density-Functional Theory of Freezing.* Phys. Rev. Lett., 1989. **63**: p. 980.

39. Xu, H., Catherine, B., *Freezing of Very Asymmetric Binary Hard-Sphere Mixtures.* J. Phys.: Condens. Matter, 1995. **7**: p. L13-L17.

40. Coussaert, T., Baus, M., *Demixing vs Freezing of Binary Hard-Sphere Mixtures.* J. Chem. Phys., 1998. **109**(14): p. 6012-6020.

41. Kranendonk, W.G.T., Frenkel, D., *Computer Simulation of Solid-Liquid Coexistence in Binary Hard Sphere Mixtures.* Molec. Phys., 1991. **72**(3): p. 679-697.

42. Denton, A.R., Ashcroft, N. W., *Vegard's Law.* Phys. Rev. A, 1991. **43**(6): p. 3161-3164.

43. Rosenfeld, Y., *Phase Separation of Asymmetric Binary Hard-Sphere Fluids: Self-Consistent Density Function Theory.* Phys. Rev. Lett., 1994. **72**(24): p. 3831-3834.

44. Baxter, *Percus-Yevick Equation for Hard Spheres with Surface Adhesion.* J.Chem. Phys, 1968. **49**(6): p. 2770-2774.

45. Zaccarelli, E., Foffi, G., Tartaglia, P., Sciortino, F., Dawson, K. A., *Binary Mixtures of Sticky Spheres Using Percus-Yevick Theory.* Progr. Colloid. Polym. Sci., 2000. **115**: p. 371-375.

46. Jamnik, A., *Spatial Correlations and Solvation Interaction in a Two-Component Mixture of Adhesive Fluids.* J. Chem. Phys., 1996. **105**(23): p. 10511-10520.

47. Kolafa, J., Nezbeda, I., Pavlicek, J., Smith, W., *Global Phase Diagrams of Model and Real Binary Fluid Mixtures: Lorentz-Berthelot Mixture of Attractive Hard Spheres.* Fluid Phase Equilibria, 1998. **146**: p. 103-121.

48. Kolafa, J., Nezbeda, I., Pavlicek, J., Smith, W., *Global Phase Diagrams of Model and Real Binary Fluid Mixtures. Part II. Non-Lorentz-Berthelot Mixtures of Attractive Hard Spheres.* Phys. Chem. Chem. Phys., 1999. **1**: p. 4233-4240.

49. Kenkare, P.U., Hall, C. K., *Phase Instabilities in Charged Hard-Sphere Mixtures. I. Binary Mixtures of Salt and Hard Spheres.* J. Chem. Phys., 1995. **103**(18): p. 8098 - 8110.

50. Kambayashi, S., Hiwatari, Y., *Theory of Supercooled Liquids and Glasses for Binary Soft-Sphere Mixtures via a Modified Hypernetted-Chain Integral Equation.* Phys. Rev. A, 1990. **42**(4): p. 2176-2183.

51. Leote de Carvalho, R.J.F., Evans, R., *The Screened Coulomb (Yukawa) Charged Hard-sphere Binary Fluid.* Molec. Phys., 1997. **92**(2): p. 211-228.

52. Stober, W., Fink, A., *Controlled Growth of Monodisperse Silica Spheres in the Micron Size Range.* J. Colloid Interface Sci., 1968. **26**: p. 62-69.

53. Imhof, A., Dhont, J. K. G., *Long-Time Self-Diffusion in Binary Colloidal Hard-Sphere Dispersions.* Phys. Rev. E, 1995. **52**(6): p. 6344-6357.

54. Rouw, P.W., Woutersen, A. T. J. M., Ackerson, B. J., *Adhesive Hard Sphere Dispersions.* Physica A, 1989. **156**: p. 876-898.

55. Penders, M.H.G.M., Vrij, A., *A Turbidity Study on Colloidal Silica Particles in Concentrated Suspensions using the Polydisperse Adhesive Hard Sphere Model.* J. Chem. Phys., 1990. **93**(5): p. 3704-3711.

56. Jansen, J.W., de Kruif, C. G., Vrij, A., *Attractions in Sterically Stabilized Silica Dispersions. III. Second Virial Coefficient as a Function of Temperature, as Measured by Means of Turbidity.* J. Colloid Interface Sci., 1986. **114**(2): p. 492-500.

57. Jansen, J.W., de Kruif, C. G., Vrij, A., *Phase Separation of Sterically Stabilized Colloids as a Function of Temperature.* Chem. Phys. Lett., 1984. **107**(4,5): p. 450-453.

58. Russel, W.B., *Phase Transition, Equation of State, and Limiting Shear Viscosities of Hard Sphere Dispersions.* Phys. Rev. E, 1996. **54**(6): p. 6633-6645.

59. Bartlett, P., Ottewill, R. H., *A Neutron Scattering Study of the Structure of a Bimodal Colloidal Crystal.* J. Chem. Phys., 1992. **96**(4): p. 3306-3318.

60. Bartlett, P., Ottewill, R. H., Pusey, P. N., *Superlattice Formation in Binary Mixtures of Hard-sphere Colloids.* Phys. Rev. Lett., 1992. **68**(25): p. 3801-3804.

61. Bartlett, P., Pusey, P. N., *Freezing of Binary Mixtures of Hard-Sphere Colloids.* Physica A, 1993. **194**: p. 415-423.

62. Dinsmore, A.D., Yodh, A. G., Pine, D. J., *Phase Diagrams of Nearly Hard-Sphere Binary Colloids.* Phys. Rev. E, 1995. **52**(4): p. 4045-4057.

63. Sanyal, S., Easwar, N., Ramaswamy, S., Sood, A.K., *Phase Separation in Binary Nearly Hard-Sphere Colloids: Evidence for the Depletion Force.* Europhys. Lett., 1992. **18**(2): p. 107-117.

64. Kaplan, P.D., Rouke, J.L., Yodh, A.G., *Entropically Driven Surface Phase Separation in Binary Colloidal Mixtures.* Phys. Rev. Lett., 1994. **72**(4): p. 582-585.

65. Kline, S.R., Kaler, E.W., *Interactions in Binary Mixtures: Partial Structure Factors in Mixtures of Sodium Dodecyl Sulfate Micelles and Colloidal Silica.* J. Chem. Phys., 1996. **105**(9): p. 3813-3822.

66. Krause, R., Arauz-Lara, J.L., Nagele, G., *Statics and Tracer-Diffusion in Binary Suspensions of Polystyrene Spheres: Experiment vs. Theory.* Physica A, 1991. **178**: p. 241-279.

67. Krause, R., D'Aguanno, B., Mendez-Alcaraz, J.M., *Static Structure Factors of Binary Suspensions of Charged Polystyrene Spheres: Experiment against Theory and Computer Simulation.* J. Phys.:Condensed Matter, 1991. **3**: p. 4459-4475.

68. Okubo, T., Fujita, H., *Phase Diagram of Alloy Crystal in the Exhaustively Deionized Suspensions of Binary Mixtures of Colloidal Spheres.* Colloid Polym Sci, 1996. **274**: p. 368-374.

69. Ulanowski, Z.J., Williams, I.R., *Optical Tweezers.* New Physics, 1996: p. 179-182.

70. Bartlett, P., *Structure of Multicomponent (Titania/Zirconia) Colloids.* Langmuir, 1998. **14**: p. 3538-3544.

71. Ocana, M., Hsu, W.P., Matijevic, E., *Preparation and Properties of Uniform-Coated Colloidal Particles 6. Titania on Zinc Oxide.* Langmuir, 1991. **7**: p. 2911.

72. Lorimer, J.P., Mason, T. J.,Kershaw, D., *Effect of Ultrasound on the Encapsulated of Titanium Dioxide Pigment.* Colloid Polym Sci, 1991. **269**: p. 392.

73. Gherardi, P., Mativejic, E., *Interactions of Precipitated Hematite with Preformed Colloidal Titania Dispersions.* J. Colloid Interface Sci., 1986. **109**: p. 57.

74. Iler, R.K., *Product Comprising a Skin of Dense, Hydrated Amorphous Silica Bound Upon a Core of Another Solid Material and Process of Making Same*, in *US Patent 2885366*. 1959.

75. Furlong, D.N., Sing, K.S.W., Parfitt, G.D., *The Preparation of Silica on Titanium Dioxide Surfaces.* J. Colloid Interface Sci., 1979. **69**(3): p. 409.

76. Herrington, K.D., Lui, Y. K., *Heat of Immersion of Modified Rutile Pigment in Water.* J. Colloid Interface Sci., 1970. **34**: p. 447.

77. Furlong, D.N., Rouquerol, F., Rouquerol, J., Sing K.S.W., *Adsorption Microcalorimetric Study of Rulite and Silica-Coated Rulite.* J. Colloid Interface Sci., 1980. **75**(1): p. 68.

78. Barringer, E.A., *Formation , Packing, and Sintering of Monodisperse TiO_2 Powders.* J. Am. Ceramics Soc., 1982. **65**: p. C-199.

79. Jean, T.A., *Effect of a Sterically Stabilizing Surfactant on the Nucleation, Growth and Agglomeration of Monosized Ceramic Powders.* Colloids and Surfaces, 1988. **29**: p. 273.

80. Visca, M., Matijevic, E, *Preparation of Uniform Colloidal Dispersions by Chemical Reactions in Aerosols.* J. Colloid Interface Sci., 1979. **68**(2): p. 308-319.

81. Look, J.L., Zukoski, C.F., *Shear Induced Aggregation during the Preparation of Titanium Alkoxides.* J. Colloid Interface Sci., 1992. **153**(2): p. 461.

82. Sato, S., Inaba, H., *Optical Trapping and Manipulation of Microscopic Particles and Biological Cells by Laser Beams.* Optical and Quantum Electronics, 1996. **28**: p. 1-16.

83. Svoboda, K., Block, S. M., *Optical Trapping of Metallic Rayleigh Particles.* Optics Letters, 1994. **19**(13): p. 930.

84. Mio, C., Gong, T., Terray, A., Marr, D.W.M., *Design of a Scanning Laser Optical Trap for Multiple Manipulation.* Review of Scientific Instruments, 2000. **71**(5).

85. van Helden, A.K., Jansen, J.W., Vrij, A., *Preparation and Characterization of Spherical Monodisperse Silica Dispersions in Nonaqueous Solvents.* J. Colloid Interface Sci., 1981. **81**(2): p. 354-368.

86. Al-Naafa, M.A., Selim, M. S., *Sedimentation of Monodisperse and Bidisperse Hard-Sphere Colloidal Suspensions.* AIChE Journal, 1992. **38**(10): p. 1618-1630.

87. Iler, R.K., *Definition of Colloidal Silica and Historical Development*, in *Surface and Colloid Science*, E. Matijevic, Editor. 1973, John Wiley & Sons.

88. Aelion, R., *Hydrolysis of Ethyl Silicate.* J. Am. Chem. Soc, 1950. **72**: p. 5705.

89. Matsoukas, T., Gulari, E., *Dynamics of Growth of Silica Particles from Ammonia-Catalyzed Hydrolysis of Tetra-Ethyl-Orthosilicate.* J. Colloid Interface Sci., 1988. **124**: p. 252.

90. Matsoukas, T., Gulari, E., *Monomer-Addition Growth with a Slow Initiation Step: A Growth Model for Silica Particles from Alkoxides.* J Colloid Interface Sci, 1989. **132**: p. 13.

91. Bogush, G.H., Zukoski, C. F. IV, *Studies of the Kinetics of the Preparation of Uniform Silica Particles through the Hydrolysis and Condensation of Silicon Alkoxides.* J. Colloid Interface Sci., 1991. **142**: p. 1.

92. Bogush, G.H., Zukoski, C.F., *Uniform Silica Particle Preparation: An Aggregation Growth Model.* J. Colloid Interface Sci., 1991. **142**: p. 19.

93. van Blaaderen, A., Kentgens, A.P.M., *Particle Morphology and Chemical Microstructure of Colloidal Silica Spheres Made from Alkoxysilanes.* J. Non-Cryst. Solids, 1992. **149**: p. 161-178.

94. Iler, R.K., *Silica Hydrosol Powder*, in *US Patent 2801185*. 1957.

95. van Helden, A.K., *Static Light Scattering of Concentrated Silica Dispersions in Apolar Solvents.* J. Colloid Interface Sci., 1980. **78**(2): p. 312.

96. van Helden, A.K., *Contrast Variation in Light Scattering: Silica Spheres Dispersed in Apolar Solvent Mixtures.* J. Colloid Interface Sci., 1980. **76**(2): p. 418.

97. Iler, R.K., *Colloid Chemistry of Silica and Silicates*. 1955, Ithaca, NY: Cornell Univ. Press.

98. Goodhew, P.J., Humphreys, F.J., *Electron Microscopy and Analysis*. 1988, London: Taylor&Francis.

99. Brinker, C.F., Scherer, G.W., *Sol-Gel Science*. 1990, San Diego: Academic Press, Inc.

100. Bergna, H.E., *The Colloid Chemistry of Silica*. Advances in Chemistry Series 234, ed. H.E. Bergna. 1994, Washington, DC: American Chemical Society.

101. Nishikawa, S., Matijevic, E., *Preparation of Monodispersed Spherical Silica-Alumina Particles by Hydrolysis of Mixed Alkoxides*. J. Colloid Interface Sci., 1994. **165**: p. 141-147.

102. Pouxviel, P.C., Boilot, J.P., Dauger,A., Huber, L., *Chemical Route to Aluminosilicate Gels, Glasses, and Ceramics*, in *Better Ceramics Through Chemistry II*. 1986.

103. Boilot, J.P., Pouxviel, J.C., Dauger, A., Wright, A., *Growth and Structure of Alumino-Silicate Polymers*, in *Better Ceramics Through Chemistry III*. 1988.

104. Banerjee, B.K., *Structural Study of Mullite Prepared from Different Systems/Source at Different Temperatures with the Aid of Physical Techniques like X-Ray and IR*. J. Indian Chem. Soc., 1989. **66**: p. 435-437.

105. Hirata, Y., Sakeda, K., Matsushita, Y., *Characterization and Sintering Behavior of Alkoxide-Derived Aluminosilicate Powders*. J. Am. Ceramics Soc., 1989. **72**(6): p. 995-1002.

106. Klinowski, J., *Nuclear Magnetic Resonance Studies of Zeolites*. Progress in NMR Spectroscopy, 1984. **16**.

107. Bronnimann, C., Zeigler, R.C., Maciel, G.E., *Proton NMR Study of Dehydration of Silica Gel Surface.* J. Am. Chem. Soc., 1988. **110**: p. 2023-2026.

108. Fitzgerald, J.J., Hamza, A.I., *Solid-State ^{27}Al and ^{29}Si NMR and ^{1}H Cramps Studies of the Thermal Transformations of 2:1 Phyllosilicate Pyrophyllite.* J. Chem. Phys., 1996. **100**: p. 17350-17360.

109. Guinier, A., Fournet, G., *Small Angle Scattering of X-Rays*. 1955: Wiley.

110. de Kruif, C.G., Rouw, P.W., Briels, W.J., Duits, M.H.G., Vrij, A., May, R. P., *Adhesive Hard-Sphere Colloidal Dispersions. A Small-Angle Neutron-Scattering Study of Stickiness and the Structure Factor.* Langmuir, 1989. **5**: p. 422-428.

111. Monson, P.A., *Solution of the Percus-Yevick Equation for a Binary Mixture using Gillan's Method.* 1984.

112. Cullity, *Elements of X-ray Diffraction.* 1978: Addison-Wesley Publishing Company, Inc.

113. Duits, M.H.G., May, R. P., de Kruif, C. G., *Small-Angle Neutron Scattering of Concentrated Adhesive Hard-Sphere Dispersions.* Langmuir, 1991. **7**: p. 62-68.

114. Yoshida, H., Yamanaka, J., Koga, T., Ise, N., Hashimoto, T., *Novel Crystallization Process in Dilute Ionic Colloids.* Langmuir, 1998. **14**(3): p. 569-574.

115. Fuh, C.B., Myers, M.N., Giddings, J. C., *Centrifugal SPLITT Fractionation: New Technique for Separation of Colloidal Particles.* Ind. Eng. Chem. Res., 1994. **33**: p. 355-362.

116. Eychmuller, A., Katsikas, L., Weller, H., *Photochemistry of Semiconductor Colloids. 35. Size Separation of Colloidal CdS by Gel Electrophoresis.* Langmuir, 1990. **6**: p. 1605-1608.

117. Trau, M., Saville D. A., Aksay, I. A., *Field-Induced Layering of Colloidal Crystals.* Science, 1996. **272**: p. 706-709.